Fascicle Scale Experimental and Computational Analyses of the Achilles' Tendon

A Thesis

Submitted to the Faculty

of

Drexel University

by

Oluseeni A. Komolafe

in partial fulfillment of the

requirements for the degree

of

Doctor of Philosophy

September 14 2010

Dedications

To my Parents:

Rhoda Omotunde Komolafe

and

Oluwole Komolafe

You have taught me to be independent in mind and person. To "march to my own drumbeat." You have taught me to work hard and intelligently. To **P**ersist in the pursuit of my inner vision, to **I**nsist and abide in the truth, and to **R**esist dishonest overtures. Most importantly, through your relentless prayers, sacrifice and support, you have lived faith, and demonstrated the true meaning of love. These are the lessons that I will forever cherish. Thank you.

"They stood looking at the line and then faced each other with tears in their eyes. They hugged, four of them around the fifth . . . It was obvious that they loved each other."

$\sim$ *The family line*

Olumide Komolafe, 1999

Acknowledgments

I have to start by acknowledging my advisor, Dr. Todd Doehring. This work will not have been possible without his guidance and support. I especially thank him for his role in refining my analytical skills through patient instruction and relentless high expectations.

I would like to thank Dr. Alan Lau, Dr. Margaret Wheatley and Dr. Kenneth Barbee for their service on my thesis committee. I was fortunate to have interacted with each one of them inside, and outside of class and I thank them for their advice, feedback and sometimes unconscious role in grooming my scientific development.

I especially want to thank my graduate advisor and committee chair, Dr. Rami Seliktar. I had the honor of being a teaching assistant for several of his classes, and was inspired by his concern and dedication to the art of instruction.

I want to say thank you to my current and previous colleagues in the CiBL group: Chung Park, Sreeram Vissapragada, Dhanush Chandrasekaran, Christopher Rock, Shankar Narayana, Sankhesh Jhaveri, Jaydev Dave, Pablo Burstein, Danielle Solomon. Thank you for your support and feedback.

I would like to thank the excellent biomed. office staff particularly Lisa Williams, Natalia Broz and Frank Kepics. Your pleasant, timely, above and beyond helpfulness was really appreciated.

Yewande. For always inspiring me with your quiet strength and dedication to your art. You were a much needed source of inspiration when I faltered. Thank you

Finally, it is impossible to list the many close friends that I made in the last 5 years. In different ways, each has helped me through this process. Whether lifting my spirits when I was down, doling out compassion and tough love in just-right measures or throwing it to the wind and providing much needed distractions. I appreciate you all. A prayer is in order... May you never rupture your Achilles' tendon. And if you already have, well, may it not happen again.

Table of Contents

List of Tables . . . vii

List of Figures . . . viii

Abstract . . . xii

1. THE ACHILLES TENDON . . . 1

1.1 Introduction . . . 1

1.2 Achilles Tendon Rupture . . . 3

1.3 Achilles Tendon Clinical Problems . . . 4

1.3.1 Tendinosis . . . 4

1.3.2 Chronic Tendinopathy . . . 4

1.4 Treatment options . . . 5

1.4.1 Conservative, non-surgical treatment . . . 5

1.4.2 Surgical treatment . . . 6

1.5 Biomechanical motivations . . . 8

1.6 Structure of thesis . . . 9

2. OBJECTIVES . . . 10

2.1 Overview . . . 10

2.2 Specific Aims and Hypotheses . . . 12

2.2.1 SPECIFIC AIM 1: . . . 12

2.2.2 SPECIFIC AIM 2: . . . 12

2.2.3 SPECIFIC AIM 3: . . . 12

3. BACKGROUND . . . 13

3.1 Summary . . . 13

3.2 Tendon Structure and Anatomy . . . 13

3.3 Overview of Tendon and Ligament Mechanics . . . 15

3.3.1 Nonlinear Elasticity Behavior . . . 15
3.3.2 Viscoelasticity . . . 16
3.4 Mathematical modeling of viscoelastic tissues . . . 20
3.4.1 Mechanical models . . . 20
3.4.2 Quasi-Linear viscoelastic theory . . . 23
4. Fascicle Scale Loading and Failure . . . 25
4.1 Summary . . . 25
4.2 Background: Fascicle Behavior . . . 25
4.3 Experimental Methods . . . 26
4.3.1 Sequential Sectioning Protocol . . . 28
4.4 Analytical Methods . . . 30
4.4.1 Marker-free Deformation Measurement . . . 30
4.4.2 Data Analysis . . . 30
4.5 Results . . . 32
4.6 Discussion: Fascicle behavior . . . 35
4.7 Conclusions: Fascicle behavior . . . 37
5. bidirectional viscoelasticity . . . 38
5.1 Summary . . . 38
5.2 Background: Bidirectional Model . . . 38
5.3 Materials and Methods . . . 40
5.3.1 Experimental Methods . . . 40
5.3.2 Analytical Methods . . . 42
5.4 Results . . . 44
5.5 Discussion: Bidirectional Model . . . 47
5.6 Conclusions: Bidirectional Model . . . 49
6. Finite Element Mesostructural Analysis . . . 50
6.1 Summary . . . 50

6.2 Introduction: F-E Analysis . . . 50
6.3 Methods and Materials . . . 51
6.3.1 Creating the volumetric model . . . 51
6.3.2 Model Assumptions . . . 52
6.3.3 Generating a 3-D finite element mesh . . . 53
6.3.4 Finite element analysis . . . 54
6.4 Results . . . 56
6.5 Discussion: F-E Analysis . . . 59
6.6 Conclusions: F-E Analysis . . . 61
7. Conclusions and Future Recommendations . . . 62
7.1 Review of Overall Goals . . . 62
7.2 Conclusion: Results . . . 63
7.3 Important Findings . . . 64
7.4 Contributions . . . 65
7.5 Limitations . . . 65
7.6 Future Directions . . . 66
7.6.1 Mathematical modeling- Meshless methods . . . 66
7.6.2 Modeling Contact . . . 67
7.6.3 Small Scale Experimental Testing . . . 67
7.7 Concluding Remarks . . . 68
Bibliography . . . 69
Vita . . . 74

List of Tables

4.1 Cross head and video measured extensibility, linear modulus, A and B values for the intact fascicle bundle and single fascicle specimen ($n = 7$). Significant difference was observed only for the moduli calculation 34

5.1 The mean values and standard deviations (n = 6) of the estimated parameters from the traditional QLV model and the bidirectional model. 44

List of Figures

1.1 Classical drawing of the intact Achilles' tendon(white band) showing its orientation in a human leg. The tendon is attached at the proximal end to the gastrocnemius muscle and distally to the calcaneous (from Gray's Anatomy). 1

1.2 Transverse magnetic resonance imaging (MRI) of a normal heel. (Left) A normal Achilles tendon (Right) A torn Achilles tendon with fluid collected at the site of the tear. (from Intermountain Medical Imaging, Boise, Idaho) 3

1.3 A MaxTrax ROM immobilization boot made by DonJoy Orthopedics. The foot is kept in a weight bearing short leg cast for 8 weeks with the foot in a gravity equinus position. (Left) An immobilization boot at maximum plantar flexion. (Right) at maximum dorsiflexion 6

1.4 The Kirschmayer core suture and cross-stitch paratenon suture repair technique [1]. (A) A skin and fascia incision is performed over the ruptured Achilles tendon. (B) The Kirschmayer core suture is used to connect the proximal and distal tendon ends in an approximate length. (C) The cross stitch suture is used on the paratenon surrounding the core suture. 7

1.5 Ma and Griffith percutaneous repair technique. Six skin incisions (three lateral and three medial) are made transverse to the Achilles tendon. The suture is criss-crossed through the tendon and tied on the tendon surface. 8

2.1 Hierarchical collagen structure of a rat tail tendon according to Kastelic et al [2] and polarized-light image of cross-section of human Achilles' tendon. In the image on the left, fibrils are the structural units of the fibers which themselves are the basic mechanical units of the tendon. 10

3.1 (A) An excised human Achilles tendon. The long, longitudinal fascicles are visible as striations in the tendon. (B) Polarized-light image of cross-section of human Achilles' tendon. (C) The individual fascicles, surrounded by endotenon are clearly delineated . . 14

3.2 A load-deformation plot of a tendon brought to failure at a constant elongation rate. Three regions are clearly delineated. In the toe region, the load increases exponentially with increasing elongation. In the second region, the relationship is linear. In the yield region, the tendon behavior is increasingly nonlinear and ends with failure. The peaks are due to rupture of individual fascicles. 16

3.3 Viscoelasticity – Stress relaxation. Top: The specimen is loaded to a constant strain value ε at $t = 0$. Bottom: The stress increases to a maximum value of κ_0 at $t = 0$ and relaxes to an asymptotic value of κ_∞. 17

3.4 Viscoelasticity – Creep. The specimen is loaded to a constant stress value (top). The specimen continues to deform (bottom) 18

3.5 Viscoelasticity – Hysteresis. (Left) The specimen is loaded, then immediately unloaded at the same strain rate. The curves indicate the tissue has a different force-extension relationship in loading and unloading. Plotted on a stress-strain axes, the area between the two curves represents the energy dissipated by the material. 19

3.6 Viscoelasticity – Preconditioning. As the number of cycles increase, the difference in the loading-unloading curves of successive cycles decrease. The relaxation curves (right) are seen to shift upward with increasing number of cycles 19

3.7 Relaxation and creep functions of (a) a Maxwell, (b) a Voigt, and (c) a Kelvin solid. 21

4.1 Specimen were cut from the midsubstance region as indicated. The specimens contain 4-6 fascicles and are approximately 15x4x1 mm. 27

4.2 Mesostructural testing system 27

4.3 Sequential sectioning protocol (A) intact specimen (B) split between fibers (C) lower fibers cut and split between remaining upper two fibers (D) final remaining fiber 29

4.4 First frame (left) and last frame (right) for the video tracked technique on the intact specimen (top) and the single fascicle specimen (bottom) The nodes are distributed in the first frame using a simple 2-D triangulation algorithm. The last frame shows the displacement path of each node tracked from the first frame to the last 32

4.5 Load response plot for a typical specimen (top) Plot of intact specimen and first split. The small difference in carried load shows that there are minimal interaction effects between adjacent fibers. (bottom) Loading plot of intact specimen and sample load after each cut. Two cuts were made in this specimen. The decrease in carried load with each cut is clearly shown 33

4.6 Average and single standard deviation stress-strain plot of the intact specimen and individual fascicle specimen 33

4.7 Average and single standard deviation stress-strain plot of the intact specimen and individual fascicle specimen 35

5.1 Entire testing protocol: The specimen was first preconditioned using 6 load-unload cycles at a strain rate of 3 mm/s. After recovery the specimen was subjected to a stretch-hold test. At the end of the test, the specimen was allowed to recover for 30 $mins$ and then the preconditioning was repeated. The ramp-hold-unload-hold testing protocol was used to characterize the bidirectional model. Introducing the hold portion after the unload phase allowed direct comparison of the different viscoelastic responses due to the loading and removal of load 41

5.2 Theoretical fit of the decimated stress-relaxation data using the traditional QLV model. The model parameters were estimated using the direct-fit method 44

5.3 The traditional QLV predictions of the specimen stress relaxation for 8 cycles of the ramp-hold-unload-hold testing protocol. The parameters of the model were estimated from a standard stress-relaxation test. The results show that the prediction of the unloading behavior is visibly poorer than the predictions of the loading behavior 45

5.4 A representative theoretical fit of the decimated ramp-hold-unload-hold data for 8 cycles. The bidirectional model was used with independent viscoelastic parameter sets for the loading response and the unloading response 46

5.5 Least squares error calculations for the traditional model and the bidirectional model. The error is plotted as a function of number of cycles. The errors of both models increase with increasing cycles, however, the bidirectional model more accurately represents the tissue behavior compared to the traditional QLV model 47

6.1 (A) An intimately connected sub-group of 16 fascicles is traced from the original high resolution cross section of a human Achilles tendon (B) the trace image is converted to an indexed, two domain dataset in MATLAB® (C) An volumetric dataset is created by stacking the 2-D image along the Z-axis 52

6.2 (A) A section of the unstructured mesh of 38,272 nodes and 187,858 tetrahedral elements. (B) The elements show a regular size gradient on the surface and through the the volume. 54

6.3 Color map of nodal displacements for uniaxial tension test. The bottom nodes (blue) are fixed and the axial displacement is applied to the top nodes 56

6.4 A color map of the Von-Mises stress distribution for an endotenon modulus of half the fascicle modulus. As expected, the fascicle stresses are much higher than the endotenon stresses. 57

6.5 Bar plots for the overall specimen, the fascicle and the endotenon. The plotted stress distributions are for four different endotenon moduli values. The endotenon modulus is expressed as a percent of the fascicle modulus. From left to right and top to bottom, they are 1%, 10%, 50% and 100% respectively. 58

6.6 Von-Mises, mean shear stress and median shear stress for the case with an endotenon modulus of 100% of the fascicle modulus. The Von-Mises plots would indicate that the endotenon stresses are higher than the overall and fascicle stresses. However, the low mean and median stresses indicate the specimen was likely not loaded to levels necessary for an accurate analysis. 59

Abstract

Fascicle Scale Experimental and Computational Analyses of the Achilles' Tendon

Oluseeni A. Komolafe

Todd C. Doehring, Ph.D.

Collagenous connective tissues like the Achilles tendon have a highly complex and intricate microstructure. Their anatomy, biomechanical load response and regional-scale material properties have been investigated in detail. Available studies on the Achilles tendon generally focus on the tissue's macroscopic behavior. Macroscopic scale studies are useful, however, despite best efforts, they remain unable to provide accurate and reproducible information on the biomechanical properties and loading behavior of the tendon's sub-macroscopic scale components. Knowledge of the tissue's biomechanical properties at these scales is critical to address the clinical problems of injury, particularly sub-failure injury, and repair. Historically, challenges of experimental testing and analytical modeling have precluded detailed analyses or studies at sub-macroscopic scales.

The objective of this work is to characterize the fascicle-scale biomechanical properties and load response of the human Achilles tendon by addressing the following three specific goals: (1) develop and implement experimental protocols for performing fascicle-scale studies of the Achilles tendon, (2) formulate a viscoelastic model to characterize the cyclic stress response of Achilles tendon fascicles and (3) model realistic fascicle deformation patterns using a 3-D computational model of the heterogeneous tendon microstructure. The experimental techniques and protocols presented can be extended to other connective tissues and structural scales. In addition to the application to sub-failure injury and repair, the results of this thesis work are applicable to microstructural models investigating localized cellular stress fields for tissue engineering applications.

Chapter 1: THE ACHILLES TENDON

1.1 Introduction

The Achilles tendon(Figure 1.1) is the large fibrous tendon in the back of the leg that attaches the muscles of the calf to the heel. Its function is to transfer forces from the calf muscles to the heel, causing a flexion moment about the ankles. This is essential for "push-off," i.e. plantar-flexion, activities such as sprinting, jumping, and climbing. Mechanically, the tendon operates as a large spring, storing energy and providing a highly efficient mechanism for force transfer.

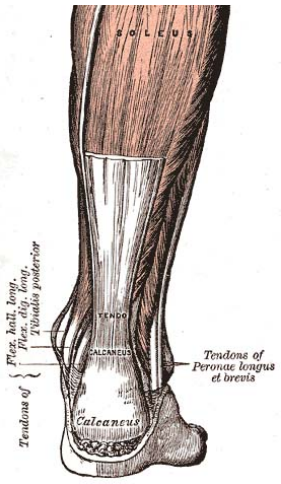

Figure 1.1: Classical drawing of the intact Achilles' tendon(white band) showing its orientation in a human leg. The tendon is attached at the proximal end to the gastrocnemius muscle and distally to the calcaneous (from Gray's Anatomy).

The tendon is named after the mythological Greek warrior "Achilles." The legend of Achilles is that the mighty and otherwise indestructible Greek warrior met his untimely death when he was mortally wounded by an arrow that struck his heel. In similar regard, although the Achilles tendon is the thickest, and arguably, strongest tendon in the human body, it is prone to sudden, painful, and catastrophic rupture. In most cases, rupture occurs without prior warning and interestingly, at loads that are significantly lower than known failure load levels of the tendon. However, the specific causes and mechanisms of failure are not well understood.

In his writings, Ambrose Pare (1510-1590), the famous French war surgeon described the first closed repair of the Achilles tendon [3]. He indicated that rupture is a common event, often caused by "a little jump, the slipping aside of the foot, the too nimble getting on horseback, or the slipping of the foot outside the stirrup in mounting into the saddle." He also noted that treatment (closed, i.e. non surgical reattachment) was ineffective, with a high rate of re-rupture. Another famous French surgeon, Jean Louis Petit (1674 - 1750) provided some of the first case reports on Achilles tendon ruptures. The earliest report of a comparative analysis of repair options was published by Quenu and Stoianovitch in 1929 [4]. They compared the recovery and re-rupture incidence of two groups of 29 patients who underwent either surgical repair, or a conservative, non-surgical repair. Although their results indicate lower re-rupture rates for the surgical repair, this study marked the start of a controversy that persists today.

The challenge to the discipline of soft tissue biomechanics is to advance knowledge of the kinetics, structural and biomechanical properties of normal and pathological tissues. Historically, studies on the mechanical and failure behavior of the Achilles tendon have focused on the bulk tissue properties using various techniques derived from classical mechanics. In recognition of the importance of structural and regional variations, recent studies have provided detailed anatomical descriptions and regional mechanical properties of the tendon. However, there remain large gaps in the body of knowledge concerning the mechanical properties and loading behavior of sub-macroscopic scale components. In particular, challenges of experimental testing and analytical modeling have precluded detailed measurements and studies at these sub-macroscopic scales. Knowledge of the tendon behavior at these scales provides crucial data required to understand the natural processes of injury and repair, develop 'function-restorative' micro-repair techniques, and accurately characterize the localized cellular stress fields necessary for tissue engineering applications.

The broad goal of this work is to advance our understanding of the normal load response behavior of the Achilles tendon, with special emphasis on structure-function relationships at the "mesostructural" i.e. fascicle scale. In the following sections, we present a clinical review of normal and pathological Achilles tendon ruptures including incidence and the available treatment(conservative

and surgical) options.

1.2 Achilles tendon rupture: Population and incidence

The Achilles tendon is reported to be the most frequently ruptured tendon in the human body, and accounts for 40% of all operated tendon ruptures [5, 6, 7]. There is a clear increase in incidence of Achilles tendon ruptures over time, from 2 in every 100,000 in 1986, to 12 in every 100,000 in 1994 [7]. Ruptures appear to occur disproportionately in men, with studies reporting male to female injury ratios ranging from a low of 2:1 to a high of 12:1 [7, 8]. Achilles tendon ruptures (Figure 1.2) typically occur during running, sprinting, jumping, and other exercises involving pushing off with the weight bearing forefoot while extending the knee joint. Peak loads ranging from 6 to 12 times the body weight have been measured during these sort of explosive contractions [9, 10].

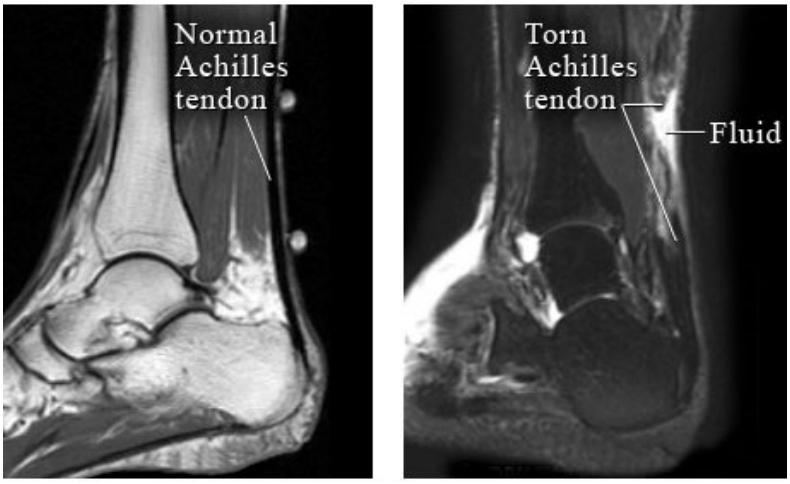

Figure 1.2: Transverse magnetic resonance imaging (MRI) of a normal heel. (Left) A normal Achilles tendon (Right) A torn Achilles tendon with fluid collected at the site of the tear. (from Intermountain Medical Imaging, Boise, Idaho)

A surprisingly large number of ruptures are reported during less intense activities, particularly in "weekend warriors." These are typically sedentary men, in their fourth to fifth decade of life, who occasionally engage in mid-level intensity exercise. The mechanisms of failure include sudden unexpected dorsiflexion of the ankle, such as occurs when slipping on a stair, stumbling, or a sudden forward fall. Other times, the tendon ruptures without any sudden overload, and without any prior warning. Clinical data indicate the following incidence due to the different failure mechanisms;

53% of ruptures occur with push-off mechanisms, 17% with sudden and unexpected dorsiflexion of the ankle(stumbling) and 10% with violent dorsiflexion of a plantar flexed foot (e.g. falling from a height) [10].

1.3 Achilles Tendon Clinical Problems

Considerable effort has been made to classify the different clinical degenerative disorders associated with Achilles tendon rupture [11]. However, occurrence of these disorders are rarely isolated, and as such, most disorders are categorized under two general processes. Tendinosis, a noninflammatory and degenerative process, and chronic tendinopathy, a condition typically marked by pain with activity and significant swelling.

1.3.1 Tendinosis

Tendinosis is a degenerative condition that predisposes a tendon to sudden and catastrophic rupture, often without any clinical symptoms. Although usually related to natural aging and failure of normal inhibitory mechanisms, this degenerative condition has been reported in much younger patients as well [9, 12]. Histology studies show a high disorganization of the collagen fibers [13, 14]. The predominant type I collagen is replaced by weaker type III collagen, and there is greater separation of the smaller diameter fibers. The degeneration generally become symptomatic with overuse and heavy training, leading to localized pain, tenderness and thickening in the tendon [11].

1.3.2 Chronic Tendinopathy

Chronic tendinopathy is a blanket term for a number of tendon overuse injuries. It is characterized by inflammation and tendon thickening. One of the most frequently occurring injuries is paratenonitis. The paratenon is a single cell layer, rich in blood vessels that nourishes and surrounds the Achilles tendon, enhancing gliding function during dynamic activity. In addition to inflammation, paratenonitis is usually accompanied by hypoxic mucoid degeneration, noduling and calcific formation. Over time, these conditions may initiate problematic fissuring within the tendon, decreasing its tensile strength [15, 16].

The combined effect of the described pathologies, training errors, muscle weakness, decreased

flexibility and biomechanical abnormalities increase the likelihood of microscopic collagen failure [17, 18, 19, 20, 21]. These micro-tears predispose the tendon to unequal distribution of tensile loads which leads to eventual tendon rupture.

1.4 Treatment Options for Achilles Tendon Injuries

The majority of Achilles tendon injuries are due to overuse, therefore, rest or modification of activity should always be part of the initial treatment. Runners are especially advised to reduce their activity level by approximately 25% once they notice soreness or tightness of the tendon. Other preemptive treatments include cold therapy, heat, massage, ultrasound, electrical stimulation, laser therapy and nonsteroidal anti-inflammatory medication [22, 23, 24, 25]. The following sections discuss the available treatment options for Achilles tendon ruptures. The treatments, limitations, and risk of re-rupture are presented.

1.4.1 Conservative, non-surgical treatment

The primary advantage of the conservative approach is elimination of wound complications and sural nerve damage during surgery. Conservative management of Achilles tendon ruptures is based on protocols involving extended periods of rigid immobilization. The injured leg is initially immobilized in a position of maximal plantar flexion, then after four weeks, the amount of plantar flexion is gradually reduced (Figure 1.3).

Figure 1.3: A MaxTrax ROM immobilization boot made by DonJoy Orthopedics. The foot is kept in a weight bearing short leg cast for 8 weeks with the foot in a gravity equinus position. (Left) An immobilization boot at maximum plantar flexion. (Right) at maximum dorsiflexion

The non-surgical treatment option can produce good functional results and remains a viable option for patients of moderate-to-low activity level or wound healing problems. Additionally, there is no risk of nerve damage, infection, or other complications of surgery. However, the conservative approach has a high risk of re-rupture, with rates from 3-20% [26, 27, 28]. Also, the long period of cast immobilization of the ankle joint leads to calf muscle weakness. This extends the recovery and rehabilitation time to full weight bearing.

1.4.2 Surgical treatment

Surgical repair of ruptured Achilles tendons is usually recommended for younger and active individuals. In a study comparing functional metrics of a leg with a repaired Achilles tendon, and the uninjured opposite side of 29 athletes [29], Mandelbaum reports no significant differences in ankle motion, isokinetic strength and endurance of both legs after 12 months of functional rehabilitation. Clinical studies also show very low re-rupture rates of 1% to 1.4% for surgical treatments of Achilles tendon ruptures [30, 31, 32]. Despite the functional benefits and low rate of re-rupture, surgical treatment is still highly controversial because of the high rates of complications. In a study of 775 patients with ruptured Achilles tendon, 20.4% of the patients treated using an "open repair" technique developed complications [27], including skin necrosis, wound infection, sural neuromas, adhesion of the scar to the skin, and the usual anesthesia risks.

Open repair

In an **open repair**, a longitudinal incision is made in the skin from the medial aspect of the heel to the calf. The paratenon(membranous tissue surrounding the tendon) is then cut in line with the tendon. Any necessary debridement of scar tissue is made, and the ends of the tendon are re-apposited. Suturing techniques include end-to-end Bunnell, Kessler or Kirschmayer sutures (See Figure 1.4 below) to more complex procedures like fascia flaps or tendon grafts.

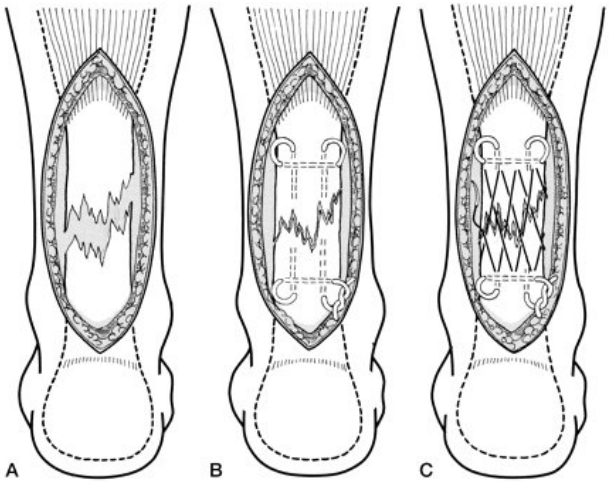

Figure 1.4: The Kirschmayer core suture and cross-stitch paratenon suture repair technique [1]. (A) A skin and fascia incision is performed over the ruptured Achilles tendon. (B) The Kirschmayer core suture is used to connect the proximal and distal tendon ends in an approximate length. (C) The cross stitch suture is used on the paratenon surrounding the core suture.

Benefits of the open repair technique include; decreased rates of re-rupture, less residual tendon lengthening, less calf atrophy and better ankle range of motion. However, there remains a high (>20%) risk of surgical complications associated with this repair.

Percutaneous surgery

The high rate of wound complications following open repair procedure prompted investigation into minimally invasive, and percutaneous surgical repair. **Percutaneous repair** techniques include the use of the Dresden instrument, the Tenolig system, and the Ma-Griffith technique(see Figure 1.5). Three small transverse incisions are made on each side of the tendon, through the skin, the tendon, and out the opposite side. The sutures are then passed through the distal and proximal ends of the

ruptured tendon while the ankle is held in maximal equinus. The sutures are then cut short and tied using a surgeons knot. Although percutaneous tendon repair successfully decreases the wound complications associated with open repair, it is complicated by the surgeon's inability to visualize the two ends of the tendon. This contributes to higher rates of sural nerve injury and re-rupture due to inadequate apposition of tendon stumps using this repair technique [33, 34, 35].

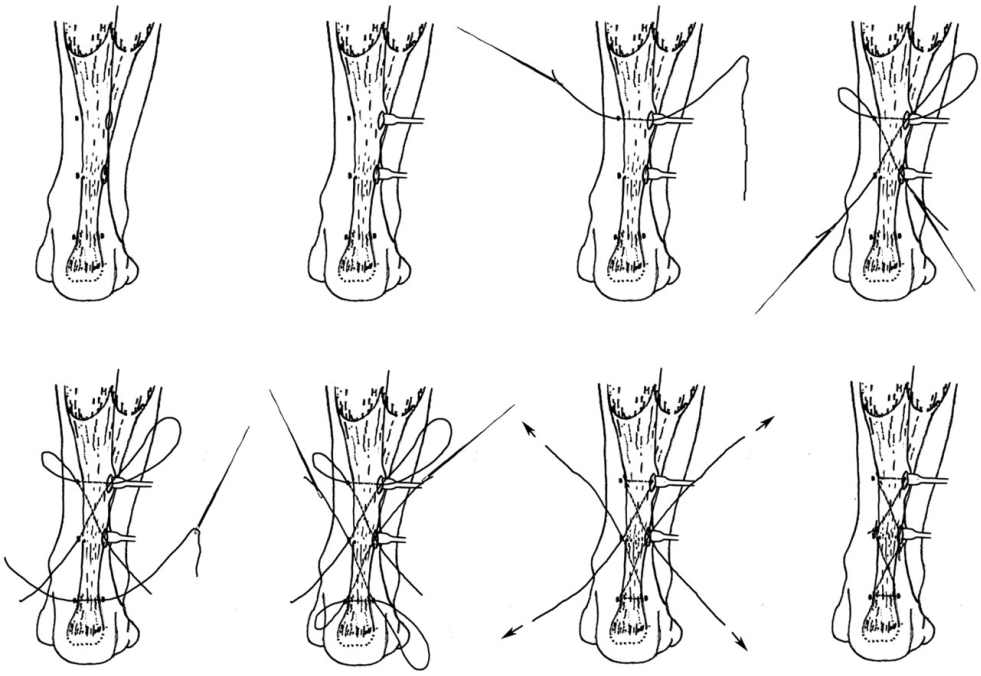

Figure 1.5: Ma and Griffith percutaneous repair technique. Six skin incisions (three lateral and three medial) are made transverse to the Achilles tendon. The suture is criss-crossed through the tendon and tied on the tendon surface.

1.5 Biomechanical motivations

Recognizing the importance and the challenges of developing accurate mechanical models of the stress behavior of complex collagenous tissues, this thesis synthesizes experimental data and analytical techniques to provide unique information on the mechanical behavior of sub-macrostructural (i.e. fascicle) scale tissue components. This knowledge provides an essential foundation for microstructural computational models of tissue behavior.

Results from the studies undertaking in this work may find use in "micro-surgical" repair of soft tissues and in the mechanical remodeling of grafts and engineered replacement tissues. Advances in

imaging technology have begun to provide highly detailed information on the complex microstructure of soft tissues. We now know that the parallel fiber model historically applied to tendons and ligaments does not accurately characterize the fiber organization. The tissues are significantly more complex; with hierarchical, interwoven fibers of varying sizes and complicated geometry. Micro-surgical repair represents a surgical paradigm shift away from the gross, end-to-end approach of repairing ruptured tissues, to a microstructural approach where the underlying fiber structure is directly considered in the repair. By providing individual fascicle, group fascicle, as well as fascicle-to-fascicle interaction data, this work represents an important first step towards developing quantitative metrics that are necessary for comparison of normal and repaired tissues.

Mechanical stimulation is a critical component in engineering load bearing tissues and conditioning existing tissues in new auto grafted roles. It is well established that mechanical loading may be used to guide the formation of new tissues from ligament and tendon fibroblasts. It is also well established that living tissues responds to altered loads through endogenous changes in its microstructural organization. Without the appropriate biomechanical cues, new tissue formation lacks the collagenous microstructure necessary to function in its load bearing role within the body. Data from the characterization of the local stress state around fascicles are useful for highly accurate predictions of the tissue's cellular stress state in different loading configurations.

1.6 Structure of thesis

The following chapters present a series of experiments, analyses and computational models. In Chapter 2, the overall objectives of this work, as well as specific aims and hypotheses are presented. Chapter 3 presents background information on the structure, mechanics and mathematical modeling approaches for viscoelastic materials. Chapters 4, 5 and 6 are studies on the three specific aims of chapter 2. Each of the three chapters is self-contained with a brief introduction, a description of the methods, discussion of the results, and a conclusion. In chapter 7, the overall conclusions of this work, its contributions to the field of soft tissue biomechanics, and recommended future studies are presented.

Chapter 2: OBJECTIVES

2.1 Overview

Tendons and ligaments are soft, collagenous tissues whose primary function is to support tensile biomechanical loads, while also providing a high degree of flexibility. The properties of these tissues are largely dependent on their collagen fiber structure. The fibers are mostly arranged in parallel, in discreet, hierarchical bundles (e.g. fascicles) that can slide relative to each other. This structure (Figure 2.1) is likely optimal from an evolutionary standpoint, allowing the tendons and ligaments to flex with minimum expenditure of energy.

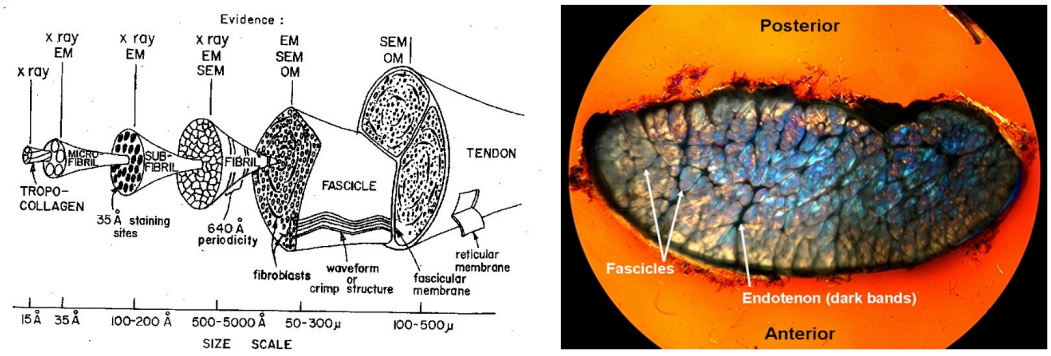

Figure 2.1: Hierarchical collagen structure of a rat tail tendon according to Kastelic et al [2] and polarized-light image of cross-section of human Achilles' tendon. In the image on the left, fibrils are the structural units of the fibers which themselves are the basic mechanical units of the tendon.

Despite this knowledge of the fiber structure, studies on tendon and ligament biomechanics have typically focused on the gross tissue mechanical behavior. This is because of the historical application of the continuum theory which was developed for analysis of relatively simple, homogeneous engineering materials. A few studies [36, 37, 38] that have attempted to account for microstructure using continuum approximations such as homogeneity theory (composite materials); however, these studies commonly assume that the fibers are fully connected and deform homogeneously, that is, in an affine sense with respect to the macroscopic deformation.

The affine assumption describes the fiber strains as a tensorial transformation of the overall tissue

strains in the direction of the major axes of the applied load. This assumption is appropriate for many engineering materials; however, studies on the loading response of Achilles' tendon fascicles and other soft biological tissues show significant fiber-to-fiber sliding(non-affine) as well as non-linearities due to the relative rotations of fascicles during loading. Mathematical models based on unrealistic affine assumptions are limited in their ability to accurately characterize the experimental behavior of these soft collagenous tissues. Accurate characterization of non-affine behavior is critical for stress calculation. This is particularly important for microstructural models attempting to predict cell-matrix stresses and inform on sub-failure injury and repair.

The overall goals of this work are (1) to perform novel fascicle-scale experiments, (2) To analyze tensile test data using novel viscoelastic models and (3) to develop a 3-D computational model of tendons that begins to account for fiber-to-fiber sliding and other non affine deformations. We describe our approach in the following four specific aims:

2.2 Specific Aims and Hypotheses

2.2.1 SPECIFIC AIM 1:

To characterize the biomechanical properties of the Achilles' tendon at the fascicle scale. We analyze the stress response of single and groups of fascicles, and quantify the interaction effects

H1.1: The stress response of single fascicles are significantly different from the average stress response of fascicle groups

H1.2 Individual adjacent fascicles in aggregate groups experience small interaction effects

2.2.2 SPECIFIC AIM 2:

Formulate a constitutive model of the fascicle-scale bidirectional viscoelastic response of Achilles tendon to cyclic loads.

H2.1 The linear elastic behavior of Achilles tendon fascicles is not significantly different in loading and unloading

H2.2 The viscoelastic stress behavior of Achilles tendon fascicles is significantly different in loading and unloading

2.2.3 SPECIFIC AIM 3:

Develop a finite element model of the Achilles tendon incorporating the internal microstructure and physiologically relevant material properties of endotenon and fascicle substructures.

H3.1 Local stresses in fascicles are significantly different when heterogeneous microstructural material properties are represented

H3.2 Fascicle load deformation behavior will be significantly different than overall tendon

Chapter 3: BACKGROUND

3.1 Summary

This chapter presents background information on (1) the anatomy and microstructure of Achilles' tendon, (2) tendon and ligament mechanics, and (3) mathematical modeling approaches of the response.

3.2 Detailed Structure and composition of the Achilles' tendon

The Achilles' tendon is longitudinally oriented along the proximodistal axis of the lower leg. It attaches the triceps surae (soleus and the two heads of gastrocnemius) to the calcaneous (Figure 1.1). The formation of the Achilles tendon from the triceps surae has been described in detail by Cummins et al. [39] "The medial and lateral heads of the gastrocnemius arise from the femoral condyles and their contribution to the Achilles tendon commences as a wide aponeurosis at the lower ends of these muscular bellies." The tendon fibers formed from the gastrocnemius converge as they descend, so that the Achilles tendon narrows, typically about 6cm above the calcaneous insertion site. The fibers also rotate around those of the soleus, so that they attach laterally at the calcaneous while the soleus fibers attach medially. This spiraling, or "twist" of the tendon fascicles results in less fiber buckling when the tendon is lax, and less deformation when the tendon is under tension.

The cross sectional shape of the Achilles tendon varies considerably along its proximodistal axis. Similar to other tendons, it flares out as it nears its bony insertion site to approximately 3cm wide and 2-3mm thick [40].

The Achilles' tendon is dominated by type I collagen(86% of tendon dry weight), which accounts for its significant tensile strength, on the order of 50 - 100N/mm [41, 42]. Studies on the microstructure of the Achilles' tendon reveal a similar hierarchical organization to that described by Kastelic [2] (see Figure 2.1). A collection of tropocollagen molecules form a collagen fibril. The fibril diameters are dependent on the animal and tissue source, but range from 20 to 40nm [43]. As the structural

unit of the tendon, the fibrils are organized into successive groups of fibers, fiber bundles and fascicles [44]. The fascicles can be long, and often appear to extend the entire length of the tendon. Adjacent fascicles are separated by a membranous endotenon (Figure 3.1) which form vascularized and innervated layers of loose connective tissue that promote independent movement between fascicles [45]. The entire tendon is surrounded by a paratenon, which together with the epitenon, "form an elastic sleeve that permits the tendon to glide relative to adjacent structures." [17] Other components include type III, V and VI collagen . Proteoglycans such as: decorin, fibromodulin, biglycan, lumican and versican in the amorphous matrix, water (60 to 70 percent by weight) and fibroblast cells are also present in the Achilles tendon [46]. The interaction of the solid components with water, as well as the inherent viscoelastic properties of the collagen fibrils, are responsible for their time and history dependent properties [47].

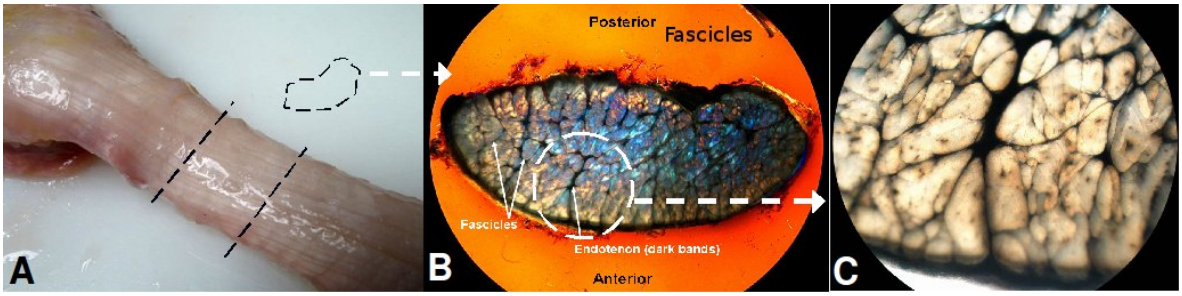

Figure 3.1: (A) An excised human Achilles tendon. The long, longitudinal fascicles are visible as striations in the tendon. (B) Polarized-light image of cross-section of human Achilles' tendon. (C) The individual fascicles, surrounded by endotenon are clearly delineated

Little is known about the etiology of Achilles tendon failure and there is currently no way to predict the potential for failure. Failure is usually sudden, catastrophic, and painful, requiring surgical repair. It is often reported to occur during normal daily activity, although this report is suspicious, since the patient may not recognize, or may wish to conceal prior overload [48]. Surgical repair with aggressive rehabilitation has been reported to be highly successful in younger patients (<50 yrs age) compared to conservative management [49]. However, the loads experienced during rehabilitation increase the likelihood of re-rupture.

3.3 General overview of tendon and ligament mechanics

The primary function of the Achilles tendon is to guide and direct motion in any activity requiring plantar-flexion of the foot; it directly affects activities like walking and jumping. Contractions of the gastrocnemius muscles pull the Achilles tendon upwards and cause rotation of the foot about the heel. Reports from studies on human Achilles tendon indicate typical walking loads of 50-60 MPa and running loads of approximately 111MPa. These values correspond to forces of approximately 3 times the body weight for walking, and 8-12 times the body weight for high velocity activities like sprinting or jumping [50].

The mechanical properties of tendons and ligaments are determined by the organization and relative quantities of their constituent fibers, cells and ground substance. Tendon fiber bundles have a more regular parallel structure, and typically contain more elastin than ligaments. As such, tendons are significantly more extensible than most ligaments. Studies indicate that soft tissues exhibit biomechanical behavior similar to the bone remodeling law described by Julius Wolff (1836-1902). The law states that injured and growing bones respond to applied mechanical forces by adapting in size and internal structure. However, unlike in bone, the mechanics and processes in soft collagenous tissues are not as well understood. Two reasons are; (1) The hierarchical microstructure of tendons and ligaments presents a highly complex problem for developing quantitative structure-function relationships, and (2) Unlike the linear load response of bones, tendons and ligaments have a complicated nonlinear and time-dependent load response.

3.3.1 Nonlinear Elasticity Behavior

Figure 3.2 is a typical load-elongation curve for a tendon loaded to failure at a constant elongation rate. This response is clearly nonlinear since the three different regions have different slopes. Normal physiological loading usually occurs in the toe region. The linear and yield regions correspond to the "reserve strength" of the tendon [43].

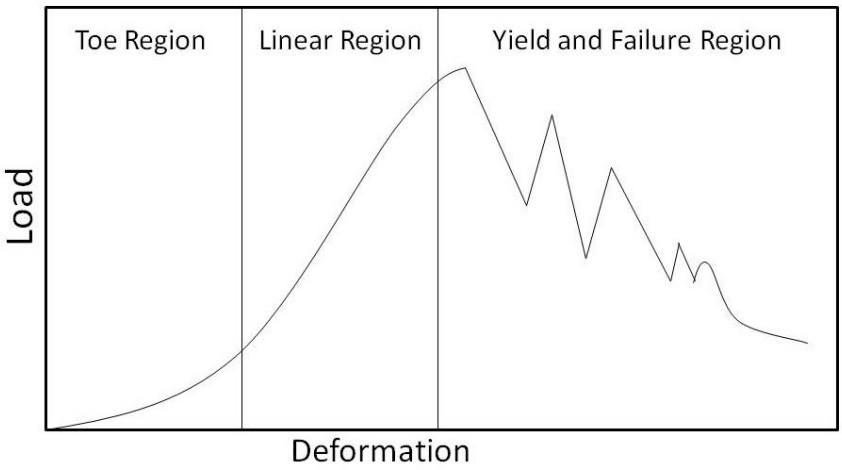

Figure 3.2: A load-deformation plot of a tendon brought to failure at a constant elongation rate. Three regions are clearly delineated. In the toe region, the load increases exponentially with increasing elongation. In the second region, the relationship is linear. In the yield region, the tendon behavior is increasingly nonlinear and ends with failure. The peaks are due to rupture of individual fascicles.

The different slopes in the regions of the load-elongation curve can be described in the context of structure-function relationships. The low stiffness of the toe region represents the straightening of the naturally wavy (i.e. crimped) collagen fibrils. This uncrimping requires very low loads, so the toe region begins with an almost flat curve. As more fibers are straightened, there is an exponential increase in the supported load by the tissue. The higher stiffness in the linear region is an average of the stiffness contributions of all the straightened fibers. Increasing the load starts to cause the stiffest fibers to fail as shown by the load decrease in the yield region. Complete rupture occurs when the remaining fibers are unable to support the applied loads.

3.3.2 Viscoelasticity

Tendons and ligaments also exhibit viscoelastic behavior i.e.the stress response of loaded tissues have a time dependent (viscous) component, and a strain-history dependent (nonlinear elastic) component. The inherent viscoelasticity of the collagen fibrils and the interaction of the solid components of the tendon with water, are responsible for their time and history dependent properties [47]. The following phenomena are characteristic of viscoelastic materials: stress relaxation, creep, hysteresis and preconditioning.

Stress relaxation

A viscoelastic material loaded at a finite strain rate and maintained at a constant deformation experiences a stress reduction, or asymptotic relaxation from the maximum value of stress to a limiting non-zero level (see Figure 3.3 below)

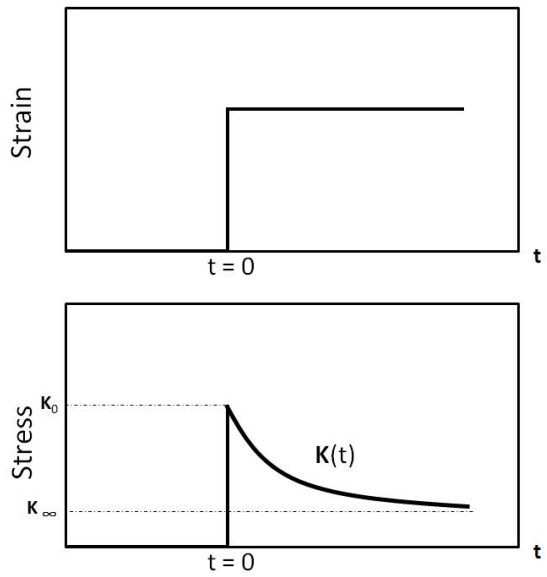

Figure 3.3: Viscoelasticity – Stress relaxation. Top: The specimen is loaded to a constant strain value ε at $t = 0$. Bottom: The stress increases to a maximum value of κ_0 at $t = 0$ and relaxes to an asymptotic value of κ_∞.

Creep in homogeneous materials

If a viscoelastic material is subjected to a finite stress that is maintained over time, the material continues to deform (figure 3.4). This is different from elastic materials which have proportional deformations for a fixed load.

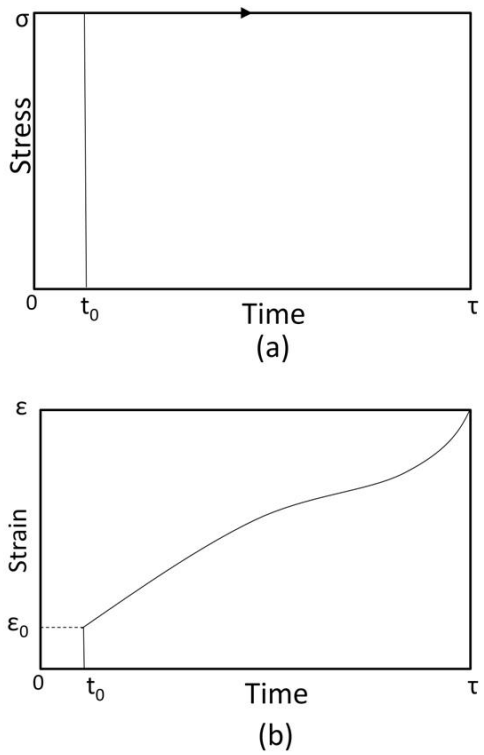

Figure 3.4: Viscoelasticity – Creep. The specimen is loaded to a constant stress value (top). The specimen continues to deform (bottom)

Creep in biological tissues

Non-homogeneous biological materials such as tendons have much more complex behavior. This is because as the tendon is loaded during creep, the tissue fibers are undergoing complex changes such as fiber recruitment and "unwinding." This unwinding is a result of rotations and uncrimping of the fibrils that make up the tendon.

Hysteresis and preconditioning

A viscoelastic material subjected to cyclic loading has different stress-strain relationship for the loading and unloading processes(figure 3.5). This phenomenon is known as *hysteresis*. The difference in area of the two curves represents the dissipated energy during loading. This is different from elastic materials which store all the energy applied during loading and release it during unloading.

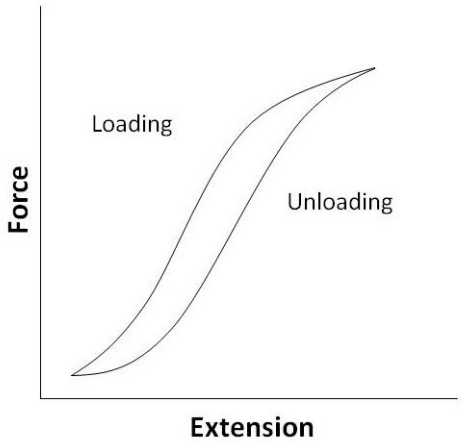

Figure 3.5: Viscoelasticity – Hysteresis. (Left) The specimen is loaded, then immediately unloaded at the same strain rate. The curves indicate the tissue has a different force-extension relationship in loading and unloading. Plotted on a stress-strain axes, the area between the two curves represents the energy dissipated by the material.

Figure 3.6 illustrates the concept of preconditioning. Subjected to repeated cyclic loading, the amount of hysteresis of viscoelastic materials is reduced and eventually, the stress-strain curves become reproducible. The stress-strain curves are seen to shift to the right with increasing cycles of loading and unloading. In theory, if the cycles are repeated indefinitely, the difference in successive cycles reduce and eventually disappear.

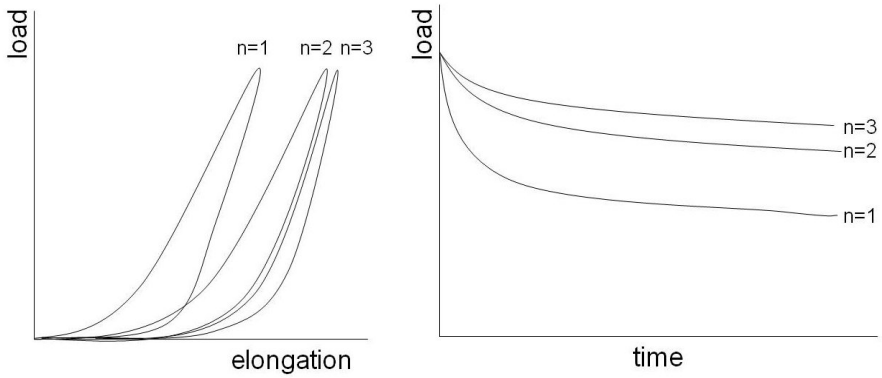

Figure 3.6: Viscoelasticity – Preconditioning. As the number of cycles increase, the difference in the loading-unloading curves of successive cycles decrease. The relaxation curves (right) are seen to shift upward with increasing number of cycles

Repeated cycling changes the internal structure of the tissue. The internal microstructure eventually reaches a near steady state conformation. Little shifting of the stress-strain behavior can be

witnessed without changing the cyclic routine. Experiments with soft collagenous tissues are usually performed on preconditioned tissues to eliminate variability effects from the internal structure.

3.4 Mathematical modeling of viscoelastic tissues

The nature of biological soft tissues pose a complicated challenge to attempts at mathematical modeling. Accurate models have to account for the time dependent and the nonlinear aspects of the tissue response. The tissues can exhibit anisotropic mechanical responses and models have to be sufficiently robust to accurately represent the tissue stress response to different loading configurations using a minimum of possible formulation parameters. Phenomenological models have been successful in reproducing the gross viscoelastic behavior of a wide range of tissues. These models are formulated using purely mathematical parameters with no direct tissue morphological basis. As such, they are very useful for characterizing tissue behavior, but are limited in their ability to relate the the constitutive and failure behavior of soft tissues to underlying composition and microstructure [51]. In this section, we explore two commonly used phenomenological models. The first is the use of mechanical analogs like springs and dashpots combined to simulate the experimental load-elongation relationship of the tissue. This approach has numerous benefits and is well developed tissue deformations of small amplitude about an equilibrium state where the theory of linear viscoelasticity applies. For large, physiological based deformations, we introduce the use of the quasi-linear viscoelastic theory. This theory is highly relevant to the work present in this document and is presented in detail.

3.4.1 Mechanical models

Mechanical models are formulated by combining linear springs of spring constant μ and dashpots with coefficient of viscosity η, to produce viscoelastic effects. Three classically used models are the Maxwell model, the Voigt model, and the Kelvin model (also called the standard linear solid). The models and their stress relaxation and creep functions are illustrated in Figure 3.7.

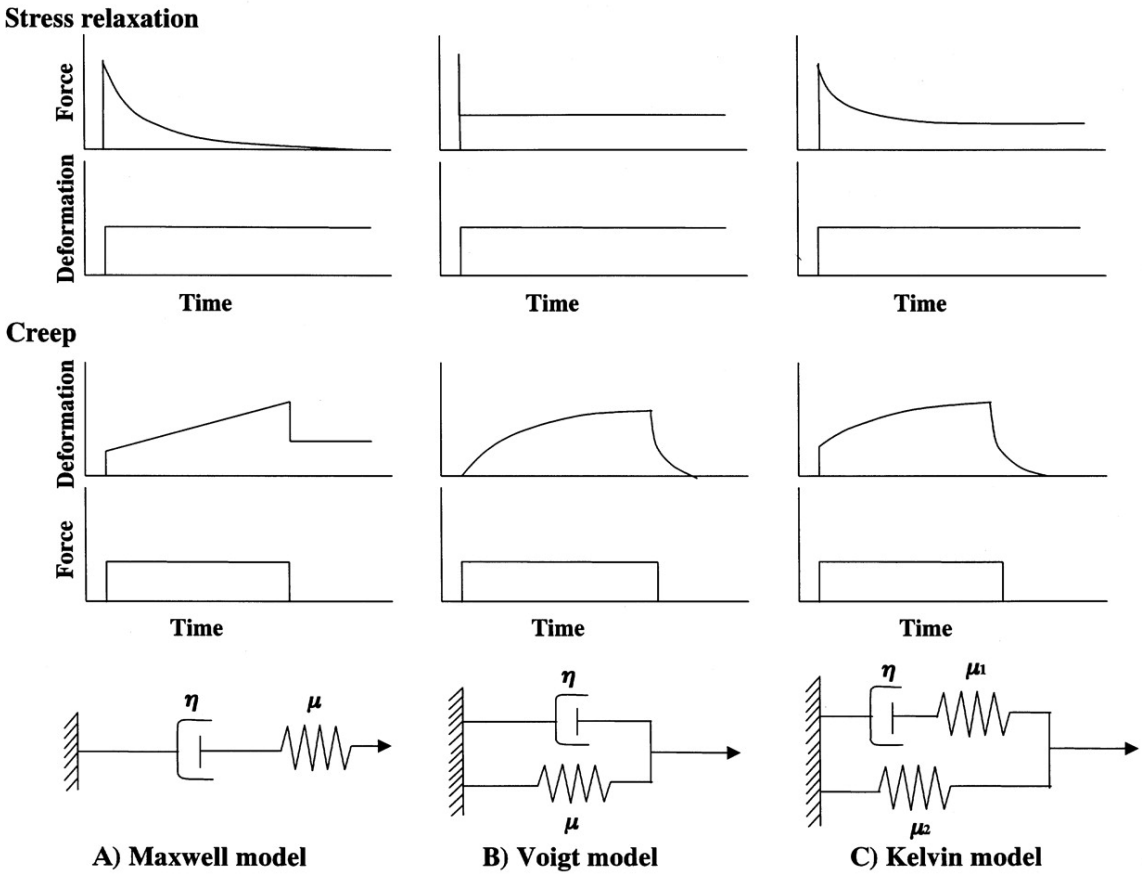

Figure 3.7: Relaxation and creep functions of (a) a Maxwell, (b) a Voigt, and (c) a Kelvin solid.

Ideally, a linear spring produces an instantaneous deformation proportion to the applied load and a dashpot produces a velocity proportional to the load at any instant. Therefore if a force F acts on spring and produces a deformation u, then $F = \mu u$. If the force F acts on a dashpot, it will produce a velocity of deformation $\dot{u}$, and $F = \eta\dot{u}$.

Maxwell model

The Maxwell analog(see figure 3.7a) is the simplest combination of elements with a spring and dashpot in series. The same force is transmitted from the spring to the dashpot. In the spring, this force produces a displacement F/μ and a velocity of F/η in the dashpot. Taking the time derivative, the velocity of the spring extension is $\dot{F}/\mu$. Summing the velocity of the spring and the dashpot, the total velocity of the system is:

$$\dot{u} = \frac{\dot{F}}{\mu} + \frac{F}{\eta} \tag{3.1}$$

If a force F is suddenly applied, the spring instantly deforms to $u(0) = \frac{F(0)}{\mu}$ but the dashpot deflection would be zero, because there will be no time to deform. Therefore, the initial condition for the Maxwell model of equation 3.1 is

$$u(0) = \frac{F(0)}{\mu} \tag{3.2}$$

Voigt model

For the Voigt model(see figure 3.7b), the spring and the dashpot are constrained to the same deformation. For a deformation u, the spring and the dashpot will produce forces μu and $\eta \dot{u}$ respectively. The total force of the system is

$$F = \mu u + \eta \dot{u} \tag{3.3}$$

If the force F is suddenly applied, the dashpot does not allow instantaneous deformation of the spring and the appropriate initial condition of equation 3.3 is

$$u(0) = 0 \tag{3.4}$$

Standard linear (Kelvin) model

The Kelvin model (see figure 3.7c) can be analyzed as a Maxwell model in parallel with a spring element. It is easily verified that the governing differential equation is

$$F + \frac{\eta}{\mu_1}\dot{F} = \mu_2 u + \eta\left(1 + \frac{\mu_2}{\mu_1}\right)\dot{u} \tag{3.5}$$

This equation can be written in the form

$$F + \tau_\epsilon \dot{F} = E_R\left(u + \tau_\sigma \dot{u}\right) \tag{3.6}$$

where

$$\tau_\epsilon = \frac{\eta_1}{\mu}, \qquad \tau_\sigma = \frac{\eta_1}{\mu_2}\left(1 + \frac{\mu_2}{\mu_1}\right), \qquad E_R = \mu_2. \tag{3.7}$$

For a suddenly applied force $F(0)$ and displacement $u(0)$, the initial condition is

$$\tau_\epsilon F(0) = E_R \tau_\sigma u(0). \tag{3.8}$$

The linear models described above are useful for basic understanding and characterization of simple materials, but are not adequate for biological tissues. To address the more complex behavior of tissues, Fung developed a Quasi-Linear viscoelasticity theory described in the following section.

3.4.2 Quasi-Linear viscoelastic theory

The basis of the Fung Quasi-Linear Viscoelastic (QLV) theory is that the instantaneous elastic, and time dependent viscoelastic responses of the tissue are independent and can be combined using a convolution integral representation. Also key to the formulation of the QLV theory is that the relaxation function has a specific continuous spectrum. Assuming a zero initial stress state, continuous elastic and reduced relaxation functions in $0 \leq t < \infty$, and the constraint $G(0) = 1$, the constitutive relationship is

$$T(t) = T^e[\lambda(t)] + \int_0^t T^e[\lambda(t-\tau)] \frac{\delta G(\tau)}{\delta \tau} \mathrm{d}\tau, \tag{3.9}$$

where t is time, $\lambda(t)$ is the time-dependent stretch, $T^e[\lambda(t)]$ is the elastic response and $G(\tau)$ is the reduced relaxation function.

For biological soft tissues, Fung proposed the use of a continuous, "box-shaped relaxation spectrum" function for $G(\tau)$. Assuming the relaxation function is the same in all directions,

$$G(t) = \frac{1 + C[E_1(\tau/\tau_1) - E_1(\tau/\tau_2)]}{1 + C \ln \tau_2/\tau_1}, \tag{3.10}$$

where $E_1(t)$ is the exponential integral function,

$$E_1(t) = \int_z^\infty \frac{e^{-t}}{t} \mathrm{d}t. \tag{3.11}$$

The QLV equation has been successfully used to characterize the viscoelastic response of a wide

variety of tissues including porcine esophagus [2], goat medial collateral ligament [46] and human anterior and posterior tibiofibular ligaments [50]. QLV parameters have often been estimated by separately fitting an exponential function of the form,

$$T^e(\lambda) = A(e^{B(\lambda-1)} - 1), \tag{3.12}$$

to the stress-strain data from the loading phase of a stress-relaxation test, and the relaxation function, of equation 3.10, to the normalized stress-time data from the relaxation phase [43, 52, 53]. The viscoelastic parameters have physical meaning: C represents the viscoelastic content of the material (i.e. the total potential for relaxation), while τ_1 and τ_2 represent time constants that govern the early and late responses of the material, respectively.

The decoupling of a tissue's stress response into independent elastic and time-dependent responses is based on the ideal condition of an instantaneous step displacement. However, experimental loading occurs at a finite time, and during ramp loading, the specimen immediately starts to relax by some unknown amount. This relaxation was not accounted for in the formulation of the QLV model and leads to erroneous parameter estimation. A number of studies have demonstrated that including the ramp displacement history could improve the accuracy of the QLV parameter estimation and the predictive ability of the constitutive model [54, 55, 56]. However, these studies required addition assumptions (i.e. extrapolations or estimations) and idealizations of the displacement ramp

The "direct-fit" method developed by Doehring, et. al. [57] is a unique method for parameter estimation that uses a global optimization algorithm to directly fit the constitutive model to the entire loading and relaxation experiment using the actual strain history as input.

The next chapter presents a detailed experimental study characterizing the biomechanical properties of the Achilles tendon at the fascicle scale. The elastic and nonlinear elastic stress response of single and groups of fascicles are reported and discussed.

Chapter 4: FASCICLE-SCALE LOADING AND FAILURE BEHAVIOR OF THE ACHILLES' TENDON

4.1 Summary

Understanding the stress response of individual fascicles is important to characterize their behavior and quantify the "interaction effects" of fascicles in aggregate groups. Individual fascicles appear loosely connected to adjacent fascicles. In the Achilles tendon, the fascicles can easily be separated from other fascicles using very small loads. This poses a significant experimental challenge to working with these specimen as they "disintegrate" upon slight handling. In this study, the mechanical properties of single fascicles and individual fascicles within aggregate bundles are investigated. Our hypotheses are that *adjacent fascicles experience small interaction effects, and that single fascicles have different mechanical properties to those of fascicle groups.* We describe a sequential sectioning protocol used to isolate single fascicles. A novel feature based algorithm is used to directly measure local specimen strains from synchronized video images of a uniaxial tensile test. The linear and nonlinear elastic mechanical properties of single and individual fascicles are compared and show a statistical ($p < 0.05$)difference.

4.2 Background: Fascicle Behavior

The structure of the Achilles tendon is likely optimized for its physiological function. A number of studies have investigated the biomechanical properties of the bulk tendon [58, 59, 60, 61]. However, there remain unanswered questions on the fascicle and sub-fascicle scale properties as well as the fascicle-to-fascicle interactions. Knowledge of the biomechanical behavior at these scales is essential to develop computational models of the tendon that can be useful for understanding, predicting and preventing failure, or developing and evaluating fascicle scale repairs.

A number of existing studies have reported the properties of fascicle-scale structures in human tendons and ligaments. The material properties from these tests vary considerably. Reports of elastic moduli range from 375 MPa to 800 MPa for the human Achilles tendon [51, 62] and from

120 MPa to 230 MPa for the human patella tendon [58, 63]. One reason for the high variability is the complexity of measuring the non-uniform cross sectional area of soft tissues. Current techniques include; various optical methods [64, 65], ultrasound imaging [66, 67] and custom designed mechanical devices [68].

Another source of variability is the experimental difficulty of measuring tissue deformation. In one study, the individual fascicles of the anterior and posterior cruciate ligament, the lateral collateral ligament and the patellar tendon of the knee were dissected along with their bony attachments, and tested in uniaxial tension [69]. The deformations were measured using the cross-head (clamp-to-clamp) data. It is acknowledged that clamp deformations do not represent actual tissue strains and this measurement has become less acceptable. A second group investigated the fascicle properties of human patellar tendon by directly clamping the individual fascicles of the human patellar to grips and testing in uniaxial tension [58]. Surface ink marks, placed 3mm away from either end of the specimen served as landmarks for recording the midsubstance deformation. This method, i.e. using surface markers, is an improvement over clamp-clamp measurements. However, in certain cases, they do not reveal the deformations of the fascicles (i.e. the main tensile load bearing structures) and represent instead, the deformation of the fascia and surrounding endotenon material. In this study, we investigate and compare the mechanical behavior of a single fascicle and a group of fascicles. Our strain calculations are based on an optical, direct measurement of specimen deformation using digital images captured during the experiment. This study provides unique data and insights on the elastic and nonlinear elastic behavior of individual tendon fascicles and fiber bundles under controlled load.

4.3 Experimental Methods

Six human (all male, 6 different individuals) Achilles tendons were dissected from their calcaneal insertion to the tendon-muscle interface. Four roughly rectangular specimens (15x4x1 mm) were cut from the midsubstance region of each tendon (figure 4.1) using a specially designed cutting tool.

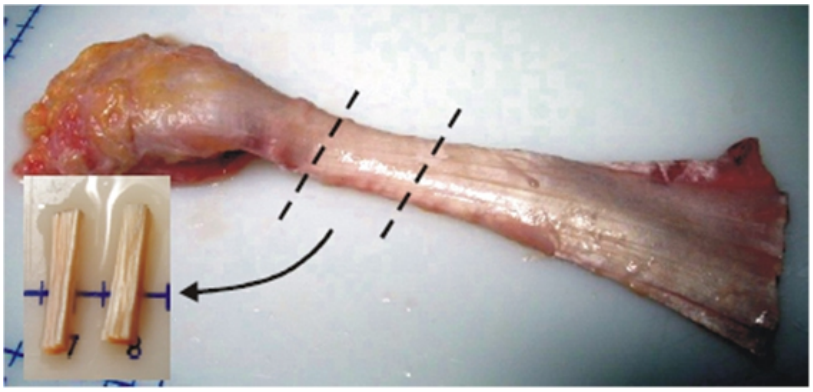

Figure 4.1: Specimen were cut from the midsubstance region as indicated. The specimens contain 4-6 fascicles and are approximately 15x4x1 mm.

The Achilles tendon contracts to a minimum cross sectional area at its midsubstance so the location of the specimens can be controlled. Each specimen contained about 4-6 individual collagen fascicles and was tested in tension on a mesostructural testing system (MSTS). "Mesostructural, qualitatively refers to structures (in this case, collagen fiber bundles) larger than cells, but smaller than the bulk tissue. The MSTS (Figure 4.2), combines tri-axial stepper-motors for controlled loading with a microscope outfitted with a synchronized imaging system.

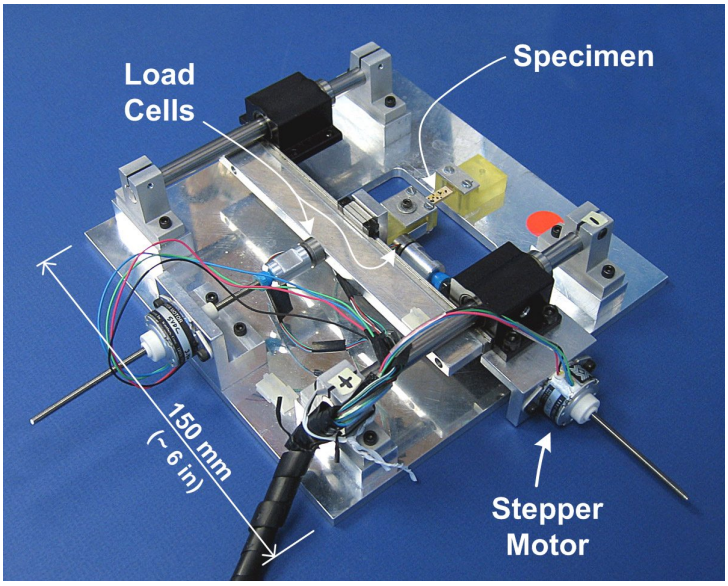

Figure 4.2: Mesostructural testing system

Although this study applies a uniaxial load to the specimen, the triaxial capability of the MSTS is useful aligning the fascicles along the loading axis. Elliptically polarized light was used to take

advantage of the birefringent property of collagen molecules and enhance the fascicle contrast, allowing the video system to capture images with clearly delineated mesostructures such as fascicles and fiber bundles. The specimens were tested using the sequential sectioning protocol described below and illustrated in figure 4.3. Note that after each loading step, the specimen was allowed to recover for 30 min. Although a 24 hour recovery time is ideal, this recovery time was determined to be sufficient for full recovery of the tissue sample following a series of preliminary studies.

4.3.1 Sequential Sectioning Protocol

1. Preconditioning: using a displacement of 1mm for 6 cycles (0.40mm/s)
2. Load to 800g (load-displacement recorded) at 0.20mm/s
3. Specimen split at fascicle boundary: load to displacement from step 2
4. One fascicle cut: load to displacement from step 2
5. Next fascicle boundary split: load to displacement from step 2
6. Next fascicle cut: load to displacement from step 2
7. Repeat 3-6, until only 1 fascicle remained
8. Load to failure: the specimen was stretched to failure, in some cases there was an audible pop.

Specimens were deformed to the exact same displacement (step 2) to ensure proper application of the principle of displacement-based superposition for the nonlinear fascicles. The linear assumption is that the total load carried by the specimen is equal to the sum of the loads carried by each individual fascicle in the specimen. This also holds for nonlinear specimens, as long as they are loaded to the same displacement, and each fiber bundle is independent (i.e. interaction effects are minimal). To ensure independence, prior to each fascicle cut, the specimen was first split between adjacent fascicles and loaded. In some cases, the interaction effects were large (defined as $> 10\%$). These cases typically indicated accidental cutting (damage) of adjacent fascicle, which on inspection, was visible under the microscope. These specimens were discarded. Generally, most fascicles could be

separated with minimal interaction effects.

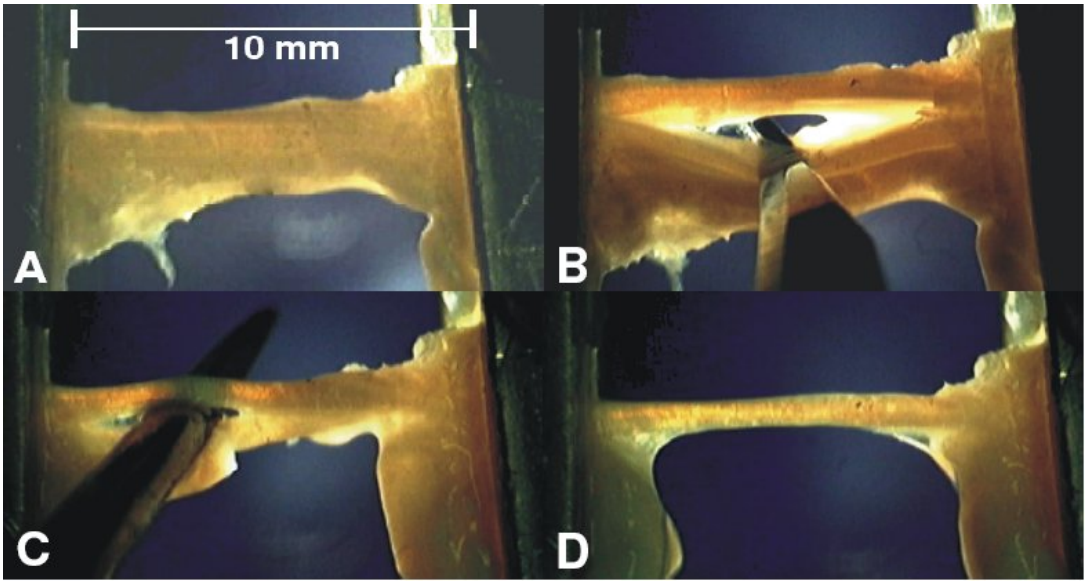

Figure 4.3: Sequential sectioning protocol (A) intact specimen (B) split between fibers (C) lower fibers cut and split between remaining upper two fibers (D) final remaining fiber

To prevent the specimen drying out during the preparation, loading and recovery phases, a drip hydration method using PBS buffer solution was used. A light meniscus (skin) of fluid was maintained over the entire specimen for the duration of the test.

Intact specimen refers to the entire excised specimen before any fascicle was cut and the strongest fascicle refers to the individual fascicle that supported the maximum load compared to all other fascicles in the same fiber bundle. The strongest fascicle for each specimen was determined by comparing the maximum loads for each fascicle. In the cases where the strongest fascicle was not the last fascicle remaining after the sequential sectioning (4 out of the 7 specimens), the loading data was obtained by subtracting the post-fascicle-cut load-cell data from the pre-fascicle-cut load-cell data.

4.4 Analytical Methods

4.4.1 Marker-free Deformation Measurement

Measurement of the specimen local deformation during loading was performed using a marker-free, feature-based, tracking algorithm programmed in Matlab (Mathworks, Inc.). The algorithm is based on the Lucas-Kanade differential method for motion estimation, described in detail by Shi [70]. The motion of features (distinct and consistent local image regions) in a sequential sequence of images is tracked using DIC. Although specimen fiber rotations are low (app. 10-20 degrees), there was a concern of the rotation potentially interfering with the calculations. The Green-Lagrange measure was used to eliminate rigid body rotations from the strain analysis. The tracking algorithm was validated by tracking color and grayscale printed patterns that represented textures similar to the specimens. Sub-pixel accuracy was achieved, equivalent to an error in strain measurement of 0.1%. Additional validation was visually performed with a frame by frame manual inspection of the tracking progress of the deformation for each specimen. The program plots the paths of motion for each point overlaying the original image, allowing visual confirmation of the tracking precision. The program also incorporates several internal checks to ensure precise tracking. For example, if a tracked point deviates more than 10% compared to its surrounding neighbors, a warning error is generated.

4.4.2 Data Analysis

Of the 24 initially excised specimens (4 samples from 6 different tendons), 9 were discarded because of procurement and handling/cutting related damages. It was necessary to establish exclusion criteria to prevent experimental induced variability in our results. The following criteria were used;

1. The specimen had to exhibit a typical nonlinear elastic load response (distinct toe and linear region)

2. The collected video had to be sufficiently high quality to allow processing of digital displacement measurement

Of the 15 remaining specimens, 8 specimens could not be tracked (optical displacement measurement) because of poor contrast, lighting or obstructions in the collected video data. The 7 remaining

specimens were accepted for final data analysis.The Youngs modulus was estimated as the slope of the tangent to the linear region of the stress-strain curve. The cross section of the fascicles was assumed rectangular. The assumed depth was maintained at 1mm and the in plane height was measured optically using a pixel-mm conversion established during calibration of the imaging system. The extensibility value was calculated as the location where the projection of line representing the linear region of the stress-strain behavior intersects with the strain axis. The nonlinear elastic behavior of the Achilles tendon was considered by constitutive modeling. Although a number of previous studies have approximated the loading behavior of soft tissues using an exponential function of the form in equation 3.12, we found in this study that a power law constitutive model of equation 4.1 provided a better fit of the loading portion of the stress strain curve. Note that for all calculations, the 2nd Piola-Kirchoff stress was used.

$$T^e(\lambda) = A(\lambda - 1)^B \tag{4.1}$$

where, λ is the time dependent stretch and T^e is the nonlinear elastic response.

A curve-fit of the elastic stress-strain data was performed using an adaptive grid refinement (AGR) global optimization algorithm previously described in detail [57]. The AGR is a robust, non-gradient based, global optimization algorithm. The strength lies in the ability to objectively determine parameters using specified parameter constraints, but without the need for an initial guess which sometimes leads to local minima solutions. This is performed by an exhaustive search that retains a small percentage of local minima parameter values of the objective function and loops back to determine the global minimal parameter set. The objective function used for the optimization was the modified chi-square error function of the form in equation 4.2

$$R^2 = \frac{1}{T^{e2}} \sum [T^e - f(\lambda(A, B))]^2 \tag{4.2}$$

The extensibility and properties (modulus, nonlinear elastic power law parameters) were determined for the single fascicle and for the intact (i.e. fascicle group) specimen. Calculations using

the clamp-clamp displacement data and the marker free digital displacement measurement data are presented to compare trends. The intact specimen and the single fascicle properties, calculated for each method, were compared using a Wilcoxon-Mann-Whitney U test for paired data with the significance level set at $p < 0.05$.

4.5 Results

The first and last tracking frame showing the DIC based tracking is presented (see figure 4.4) for the intact specimen (top) and the single fascicle (bottom). The nodes were distributed within the region of interest using a simple 2-D triangular mesh generation algorithm. All calculations were performed using displacement data from the clamp-to-clamp data as well as measurements from the DIC based video system.

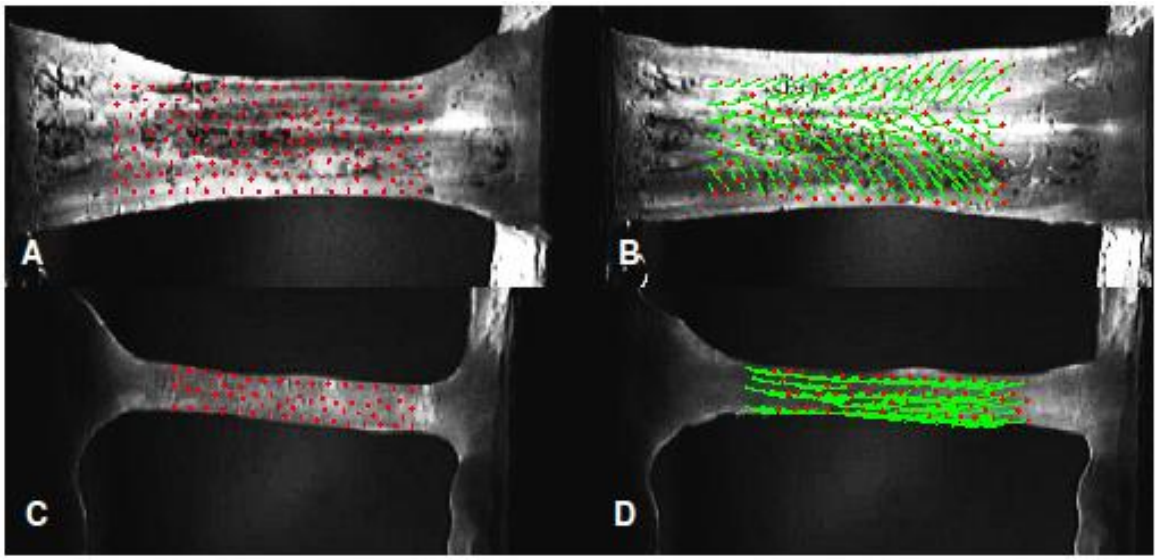

Figure 4.4: First frame (left) and last frame (right) for the video tracked technique on the intact specimen (top) and the single fascicle specimen (bottom) The nodes are distributed in the first frame using a simple 2-D triangulation algorithm. The last frame shows the displacement path of each node tracked from the first frame to the last

Analysis of video data did not show clamp slippage. The video data showed that for each specimen, distinct fascicles could be delineated using the polarized light visualization technique. Splitting adjacent fascicles resulted in only small (<10%) reductions in the carried tensile loads, however, cutting fascicles resulted in large reductions (Figure 4.5).

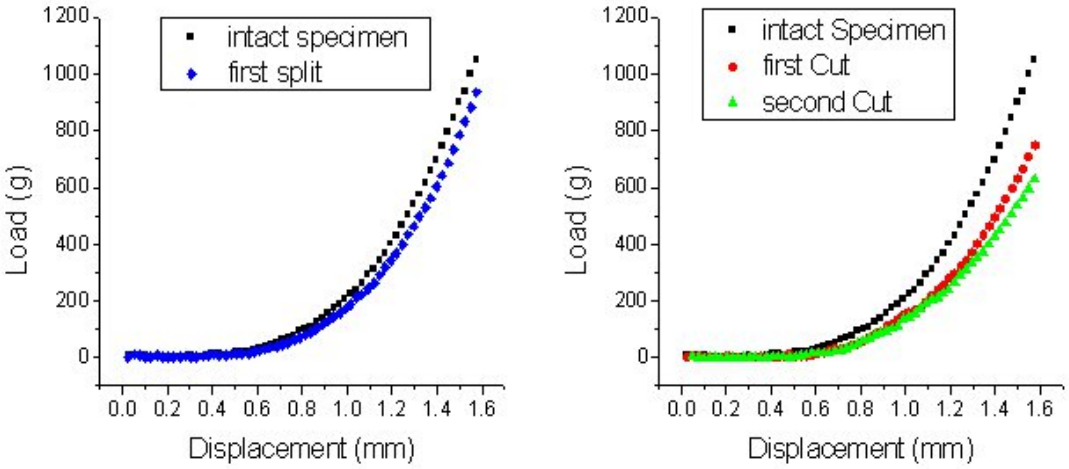

Figure 4.5: Load response plot for a typical specimen (top) Plot of intact specimen and first split. The small difference in carried load shows that there are minimal interaction effects between adjacent fibers. (bottom) Loading plot of intact specimen and sample load after each cut. Two cuts were made in this specimen. The decrease in carried load with each cut is clearly shown

The effect of the rotation of fascicles and the naturally crimped geometry of the microstructure contribute to the extended toe region in the load-displacement response. After the initial rotations were complete and all the fascicles were straightened, the stress-strain response formed a short transition, and then was nearly linear (figure 4.6).

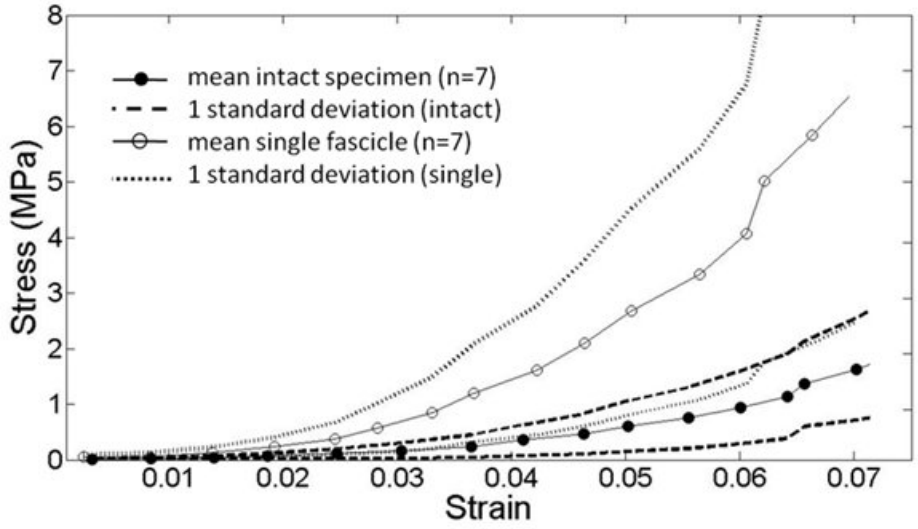

Figure 4.6: Average and single standard deviation stress-strain plot of the intact specimen and individual fascicle specimen

The average moduli values from the clamp-to-clamp data was 58.8 MPa (SD, 13.1) for the intact specimen and 113 MPa (SD, 34.8) for the single fascicle. The moduli calculated using the displacements from the video system was 68.0 MPa (SD, 33.0) for the intact specimen and 226 MPa (SD, 179) for the single fascicle. The extensibility values and the nonlinear parameter values of the power law fit (equation 4.1) are presented in Table 4.1.

		Intact fiber bundle				Single fascicle			
		extensibility(mm)	modulus (Pa)	A	B	extensibility (mm)	modulus (Pa)	A	B
cross-head	mean	0.04	5.88E+07	1.54E+09	2.51	0.04	1.13E+08	2.58E+09	2.41
	stdev	0.01	1.31E+07	8.85E+08	0.26	0.01	3.48E+07	1.98E+09	0.34
videotracked	mean	0.05	6.80E+07	2.84E+10	3.02	0.04	2.26E+08	2.51E+11	2.77
	stdev	0.03	3.30E+07	6.73E+10	0.72	0.02	1.79E+08	6.16E+11	0.82

Table 4.1: Cross head and video measured extensibility, linear modulus, A and B values for the intact fascicle bundle and single fascicle specimen ($n = 7$). Significant difference was observed only for the moduli calculation

A paired Wilcoxon-U test indicated that the modulus of the single strongest fascicle was significantly ($p < 0.05$) higher than that of the intact specimen for both the clamp data and the DIC video data. There was no significant difference ($p > 0.05$) in the A and B parameter values of the intact specimen and the single strongest fascicle for both the clamp data and the video data. Time-lapse images of the failure test showed that failure appears to initiate within a subset of the fibrils of a fascicle, followed by fascicle sliding (Figure 4.7). This was clearly visible in all failure images.

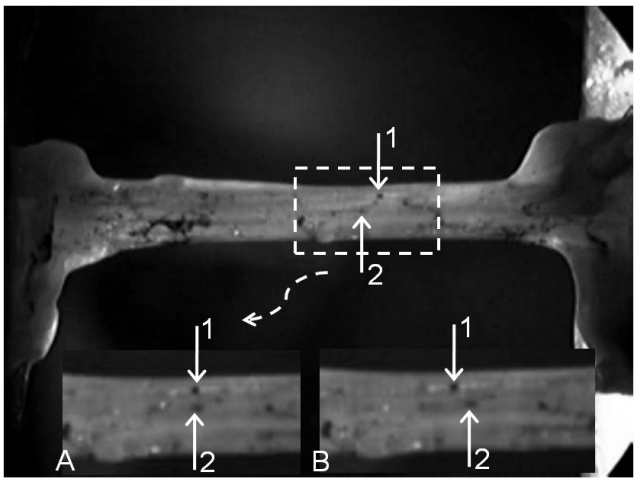

Figure 4.7: Average and single standard deviation stress-strain plot of the intact specimen and individual fascicle specimen

4.6 Discussion: Fascicle behavior

In this study, we use a sequential sectioning protocol and an optical DIC based deformation measurement algorithm to investigate the biomechanical properties of individual Achilles tendon fascicles and their interactions. To our knowledge, the biomechanical properties of human Achilles tendon at this intermediate mesostructural scale have not previously been reported. We find from the DIC based method; the modulus of the strongest fascicle was on average, 3.5 times that of the intact specimens. Some fascicles were even stronger, up to 5 times the intact specimen. These consistently higher moduli values of the strongest fascicle, as well as the observed load distribution, indicate that the overall response of the tendon may be dominated by a subset of "strongest fascicles". Indeed, the higher overall values found using the DIC method were more consistent with biomechanical properties of similar tissues reported in the literature.

We find in this study that the linear analysis (moduli) has a higher sensitivity to the differences between the intact specimen and the single fascicle than the nonlinear analysis (constitutive power law). At a probability value of 5%, we find that there is not a significant difference in the nonlinear elastic behavior of the two specimen groups. During loading, the fascicles initially rotated into the direction of loading. These rotations could be the result of forcing the specimen out of its optimal in-situ alignment (clamping effects, etc.), but they also could be present in-vivo. Small loads are

carried during rotation, even when the fibers are not tensed. We made every effort to select the gage length after large rotations were complete and the specimen was carrying load. Rotation could, however, be removed in future analysis using 3-D imaging techniques with regional analysis of the specimen: only the straightened portions of the specimen would be considered "loaded".

The use of elliptically polarized light allowed direct observation of internal structural phenomena related to loading and failure. Relative sliding of the fascicles occurred after initial failure, showing that loads were supported by a combination of the sliding mechanism and some other more elastic structure that was elongating with the fibers (such as elastin, or endotenous tissue). This result appears to be in accordance with the study by Screen [71] who reported pre and post-failure fiber sliding in a micro analysis of rat tail tendon specimens.

We note the following limitations of our results. (1) Although the use of elliptically polarized light offers significant improvements in visualization, it does not perfectly resolve intimately connected fascicles. Our single fascicles may not be individual fascicles, however, it is likely that such intimate fascicles may be tightly crosslinked and function similar to a single large fascicle. (2) The last remaining fascicle always underwent more loading repetitions (up to 3) than the first sectioned fascicle. Since the sequential cuts are arbitrarily made, the strongest fascicle was analyzed in random order (sometimes it was first cut, sometimes last). Therefore the repeated loading should not affect the results of the study. (3) Determining the exact cross-sectional area of individual fascicles in situ was challenging. We found that the fascicles have highly variable size and cross section. Some are 'rounded, approximately trapezoidal, some are triangular and a few are elliptical. Our calculations are based on a simple rectangular estimate of the cross-sectional area. However, we may be overestimating the cross-sectional area of the fascicles since we do not take into consideration the rounded vertices. (4) We have strong evidence (using elliptically polarized light) that the internal features digitally analyzed using the DIC method are the tendon fascicles. However, our measurements cannot be independently validated because (to our knowledge) there is no other way to measure the fascicle deformations of fresh intact specimens. In addition to validations confirming the accuracy of DIC deformation measurement [72], we also performed frame-by-frame manual inspection of all

DIC results to confirm marker/feature correspondence.

4.7 Conclusions: Fascicle behavior

This study achieved the goal of local characterization of the stress response of human Achilles tendon fascicles. We successfully estimated the material properties of individual fascicles, and found the moduli of single fascicles to be as high as 3-5 times the fascicles within intact specimen. However, physical separation of the membrane and crosslinks between fascicles did not lead to an equally significant reduction in the maximum load carried by the specimen. These results are puzzling, but likely amplify the importance of other load supporting, sub-macroscopic components of the tissue. Subsequent analysis will utilize a finite element simulation to investigate the role of the endotenon, i.e. reticular membrane surrounding each fascicle. This knowledge is essential for accurate computational models of the tendon that incorporate fascicle-scale behavior.

Chapter 5: LOADING AND UNLOADING OF ACHILLES' TENDON SPECIMENS: EXPERIMENTS AND A NEW BIDIRECTIONAL QUASI-LINEAR VISCOELASTIC MODEL

5.1 Summary

In this chapter, we present a constitutive model that characterizes the viscoelastic response of Achilles tendon fascicles to cyclic loads. During normal daily activities such as walking or stair climbing, tissues are subjected to alternate loading and unloading conditions. The parameters of current viscoelastic models are typically determined using the tissues response to load, and then mirrored for the unloading response. However, these models generally produce very poor characterization of the unloading behavior especially for later cycles of a load-unload test. *We hypothesize that the tendons viscoelastic stress response to loading is different from the viscoelastic stress response to an unloading boundary condition.* To test this hypothesis, we modify the Fung Quasi-Linear Viscoelastic(QLV) constitutive equation and develop a directionally dependent viscoelastic model. We compare the predictions of the traditional, symmetric Fung QLV model and the bidirectional QLV to the data from Achilles' tendon fascicle groups subjected to a novel loading and unloading testing protocol. Our results show that by independently representing the loading and unloading viscoelastic responses of the tissue, the bidirectional model provides a significantly better characterization of the experimental data.

5.2 Background: Bidirectional Model

The nonlinear and time-dependent properties, characteristic of viscoelastic materials, are critical to the physiological functioning of soft tissues. For connective tissues such as tendons and ligaments, understanding these properties and their contributions to biomechanical behavior is essential to the development of computational models of the tissues stress response. Accurately formulated models can closely represent the in-vivo behavior of the tissues, and may provide useful quantitative assessments of surgical repair and rehabilitation. A number of studies have focused on the tissues response

to applied loads, using well established protocols for stress-relaxation and creep experiments. Some of these studies successfully used the Fung Quasi-Linear Viscoelastic (QLV) constitutive equation to characterize the viscoelastic behavior of a wide variety of soft tissues, including porcine esophagus [73], goat medial collateral ligament [74] as well as human anterior and posterior tibiofibular ligaments [75]. A few studies [73, 56, 59, 57] have used the Fung QLV equation to model soft tissues responses to cyclic loads. These loading conditions are physiologically relevant; activities of daily living are usually cyclic in nature. In a typical gait cycle, every loading phase is followed by a subsequent unloading phase. Other non-ambulatory motions, particularly around the joints, usually involve multiple tissues, or multiple fiber bundles, in various loaded and unloaded states. An important assumption made in these studies is that the viscoelastic stress responses to loading and unloading are mirrored, and can be modeled using the same parameter sets.

The studies report that the Fung QLV model does not accurately predict the complete cyclic response of soft tissues, and suggest different viscoelastic stress responses to loading and unloading. Typically, the peak stresses are predicted with high accuracy, however, the valley stresses are consistently underestimated. Remarking on the results, Johnson [59] concludes that "since the cyclic test is not used to find the parameter values, failure of the parameters to describe the cyclic response indicates that either the model is inappropriate or the parameter values do not accurately describe the viscoelastic behavior of the tissue. The inability to accurately represent the tissues unloading response is likely a significant source of errors in existing models of soft tissue biomechanical responses. To our knowledge, no studies have investigated the viscoelastic stress behavior of tissues after unloading.

The goal of this study is to characterize the viscoelastic stress response of the Achilles tendon fascicle groups after unloading. In addition to improving existing computation models of tissue behavior, this work will contribute basic to the basic understanding of the mechanism of tissues responses to loads. During most physical activities, the unloading response (i.e. recovery) occurs immediately prior to loading. It is likely that the recovery behavior directly affects the tissues load response. Our working hypothesis is that different underlying mechanisms are responsible

for the tissues different responses to loading and unloading. We develop a novel testing protocol that combines elements of a stress-relaxation and a cyclic test. The protocol allows independent examination of the viscoelastic relaxation and recovery after loading and unloading. We formulate a model of the complete cyclic response by extending the one-dimensional Fung QLV model from a symmetric model to a bidirectional QLV model with a load-direction switching criterion. All parameters are determined using the direct-fit technique developed by Doehring [57]. This method directly fits a constitutive model to the exact point wise stress-time history of the test thus avoiding any assumptions or complex idealizations of the experimental stretch history.

The results of this study show that the bidirectional QLV model provides a more accurate characterization of Achilles tendon fascicle groups experimental stress response to cyclic loads than the Fung QLV model. Results of this study are likely only valid for connective tissues in tensile loading, however, they provides valuable information directly applicable to finite element, or other computational models of tissue structures in complex load/unload conditions.

5.3 Materials and Methods

5.3.1 Experimental Methods

Specimen details

Six human Achilles tendons (all male, 6 individuals) were dissected from the tendon/muscle interface to the calcaneal insertion site (figure **??**) and freshly frozen. Four 15 mm long specimens were cut from the mid-substance (central) region of the tendon (figure 4.1). Each specimen (approximately 4x1 mm rectangular cross section) contained 4-6 fascicles.

Testing protocol

Uniaxial tensile test were performed on an in-house developed mesostructural testing system (MSTS) [72]. Mesostructural qualitatively refers to structures (in this case, collagen fiber bundles) larger than cells, but smaller than the bulk tissue. The MSTS (figure 4.2), combines tri-axial stepper-motors for controlled loading with a microscope outfitted with a synchronized imaging system. Although this study applies a uniaxial load to the specimen, the triaxial capability of the MSTS is useful for aligning the fascicles along the loading axis.

Fung QLV: ramp-hold

The specimen was first preconditioned using six cycles (load-unload) at a maximum displacement of 1 mm. The specimen was returned to the original pre-load length and allowed to recover for 30 $minutes$. Preliminary experiments had determined 30 $minutes$ to be sufficient recovery time for the specimens to return to its original pre-experiment state. After 30 $minutes$, the specimen was subjected to a ramp-hold loading test; the specimen was loaded to 1000 g at a displacement rate of 7 mm/s. The displacement was recorded and maintained during the hold phase for 150-200 $secs$, by which time the specimen had relaxed to a constant stress value.

Bidirectional model: ramp-hold-unload-hold

After complete recovery (30 $mins$), the specimen was subjected to a ramp-hold-unload-hold testing protocol. The specimen was first loaded to 1000 g. The corresponding displacement was recorded and held for 20-50 $seconds$. The specimen was then unloaded to 200 g, the corresponding displacement recorded and also held for 20-50 $seconds$. The same displacement rate (3 mm/s) was used for loading and unloading. This "single cycle of ramp-hold-unload-hold was repeated for 10 times for each specimen. The entire testing protocol of each tissue sample is presented in figure 5.1.

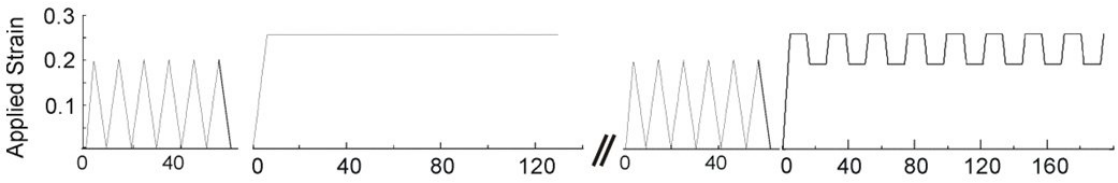

Figure 5.1: Entire testing protocol: The specimen was first preconditioned using 6 load-unload cycles at a strain rate of 3 mm/s. After recovery the specimen was subjected to a stretch-hold test. At the end of the test, the specimen was allowed to recover for 30 $mins$ and then the preconditioning was repeated. The ramp-hold-unload-hold testing protocol was used to characterize the bidirectional model. Introducing the hold portion after the unload phase allowed direct comparison of the different viscoelastic responses due to the loading and removal of load

Data acquisition and pre-processing Sampling, decimation, gage length

Loads were acquired using a low cost data acquisition system (model U12, Labjack, Inc). A simple operational amplifier circuit was used to provide a 1000x amplification of the load cell output. To

capture the fast load and relaxation response, a high data acquisition was used: 1 KHz for the first 5seconds, then 5 Hz for the remainder of the test. After collection, a simple moving average (subset of 2) was used to reduce the high frequency component of the data. To speed up the optimization algorithm, the data had to be reduced (via decimation) before processing. The decimation technique used is based on normalized equal distances along the length of the stress-relaxation curve [57]. To maintain the characteristics of the raw data, the data at all inflection points was preserved. The gage lengths were consistently determined using the following three criteria; first the load threshold was set to 4 g, second, the slope of the loading data had to show a significant increase and third, there was a visible straightening of the specimen confirming initiation of loading. The third criterion was confirmed visually using available video images collected during the experimental test.

5.3.2 Analytical Methods

Fung QLV model - Direct fit adaptation

The Fung QLV model has previously been described in detail [57, 76, 43]. The QLV parameters are traditionally estimated using nonlinear least squares curve-fits to separately fit an exponential function to the stress-strain data from the loading phase of a stress-relaxation test and a reduced relaxation function to the normalized stress-time data from the relaxation phase. We achieved the best fits of the nonlinear response using the power law of equation 4.1. Our final QLV model was as follows:

$$T(t) = A[\lambda(t) - 1]^B + AC \int_0^t [\lambda(t-\tau) - 1]^B \frac{1}{\tau} \left(\frac{e^{-\tau/\tau_1} - e^{-\tau/\tau_2}}{1 + C \ln(\tau_2/\tau_1)} \right) \mathrm{d}\tau, \tag{5.1}$$

where $(A, B, C, \tau_1, \tau_2)$ are the five constants representing the material parameters for a particular tissue.

To estimate the parameters of equation 5.1, we adopt the direct-fit method developed by Doehring [57]. The direct-fit method uses a global optimization algorithm to directly fit the constitutive equation to the entire loading and relaxation experiment. The exact, point-wise strain history is used as input in a numerical fit of the QLV constitutive equation. No additional assumptions, extrapolations or idealizations of the ramp displacements are required and in theory, any input stretch can be used for parameter estimation.

Bidirectional model Formulation and optimization

The bidirectional model extends the degrees of freedom of the traditional model and consists of two independent viscoelastic parameter sets; one for loading and the other for unloading. The final model consists of two independent parameter sets governed by a load-direction switching criterion;

$$T(t) = \begin{cases} T(A, B, C_p, \tau_{1p}, \tau_{2p}) & \text{if } \frac{\mathrm{d}\lambda}{\mathrm{d}x} > 0, \\ T(A, B, C_n, \tau_{1n}, \tau_{2n}) & \text{if } \frac{\mathrm{d}\lambda}{\mathrm{d}x} < 0, \\ no \quad change & \text{if } \frac{\mathrm{d}\lambda}{\mathrm{d}x} = 0. \end{cases} \tag{5.2}$$

where the parameters model the tissue response to loading and parameters model the response to unloading. The accuracy of the parameter estimates is dependent on the optimization method used to fit the data. In this study we use a commercial global optimization routine in Mathematica™ (Wolfram Research Incorporated, Champagne, IL). The specific optimization was a robust, derivative free, hill climbing algorithm for constrained and unconstrained nonlinear functions. An objective function was first defined as;

$$LSerror = \sqrt{\frac{\sum_1^N [T_{model}(A, B, C, \tau_1, \tau_2, \lambda(t_N)) - T_{data}(t_N)]^2}{\sum_1^N T_{data}(t_N)^2}} \tag{5.3}$$

where T_{model} is the stress calculated using equations 5.1 or 5.2, and T_{data} is the experimental stress-strain data at the decimated time points. Our parameter bounds are based on previous studies and by trial and error. A multiple start approach is used to find the global minima within the parameter bounds. To ensure that the parameters were not restricted by the boundaries, in the few cases where an optimal solution was found with a parameter "leaning" against the limits of the bound, the particular bound was adjusted and the optimization restarted. We did not find any significant differences in the loading and unloading nonlinear elastic parameters of the bidirectional model. To simplify our optimizations, we estimate the nonlinear elastic parameters of the loading response, and use the same fixed values in the unloading parameter set.

5.4 Results

We estimated the parameters of the Fung model and the bidirectional model using a fairly narrowly constrained optimization. As such, no direct comparisons can be made between our parameter and reported parameters values in the literature.

		A	B	C^*/C_p	τ_1^*/τ_{1p}	τ_1^*/τ_{1p}	C_n	τ_{1n}
Trad. QLV (*)	mean	4.16E+09	2.74	9.93E-02	6.39E-01	3.27E+03	n.a	n.a
	stdev	1.64E+09	0.20	4.19E-02	2.67E-01	2.67E+03	n.a	n.a
Bidirect. Model	mean	3.74E+09	2.70	1.04E-01	6.47E-01	2.91E+03	4.15E-02	7.25E-04
	stdev	1.69E+09	0.15	4.89E-02	2.33E-01	1.63E+03	2.30E-02	1.61E-03

Table 5.1: The mean values and standard deviations (n = 6) of the estimated parameters from the traditional QLV model and the bidirectional model.

Despite this, it is expected, and the results show (see Table 5.1) that the parameters of the Fung model and the loading parameters of the bidirectional model are not significantly different. Both parameter sets are estimated using similar stress-relaxation test. There is a significant difference (students t-test, $n = 6$, $p < 0.05$) between the parameters of the Fung model and the unloading parameters of the bidirectional model. The unloading parameters are estimated from what we refer to as an unload-hold test.

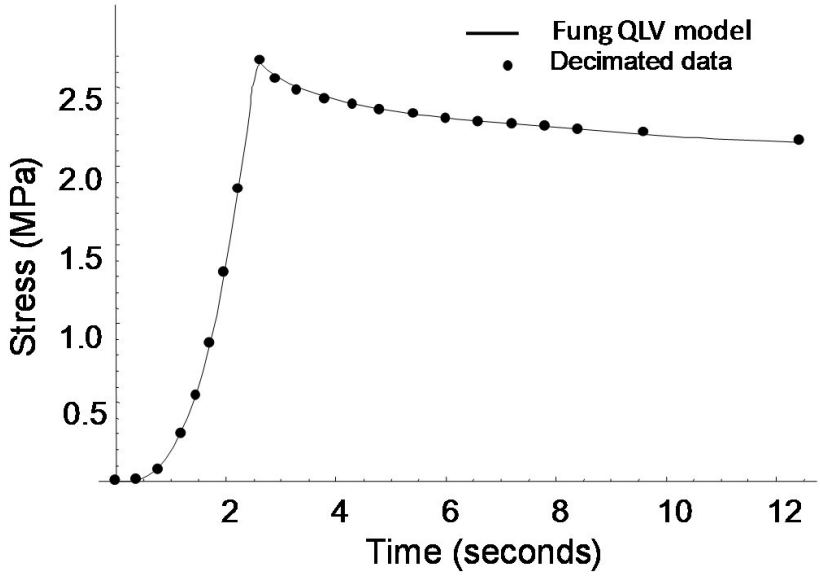

Figure 5.2: Theoretical fit of the decimated stress-relaxation data using the traditional QLV model. The model parameters were estimated using the direct-fit method

The direct fit method consistently provided good characterizations of the stress-relaxation data (figure 5.2). The estimated parameters were used to predict the stress response to all 8 cycles of the load-hold-unload-hold protocol (figure 5.3). The Fung model accurately predicted the stress relaxation response of the first load phase. By the first unloading phase, it is clear that the Fung model provides a poor fit of the unloading data. This error compounds, and subsequent loading and unloading cycles are also poorly fit.

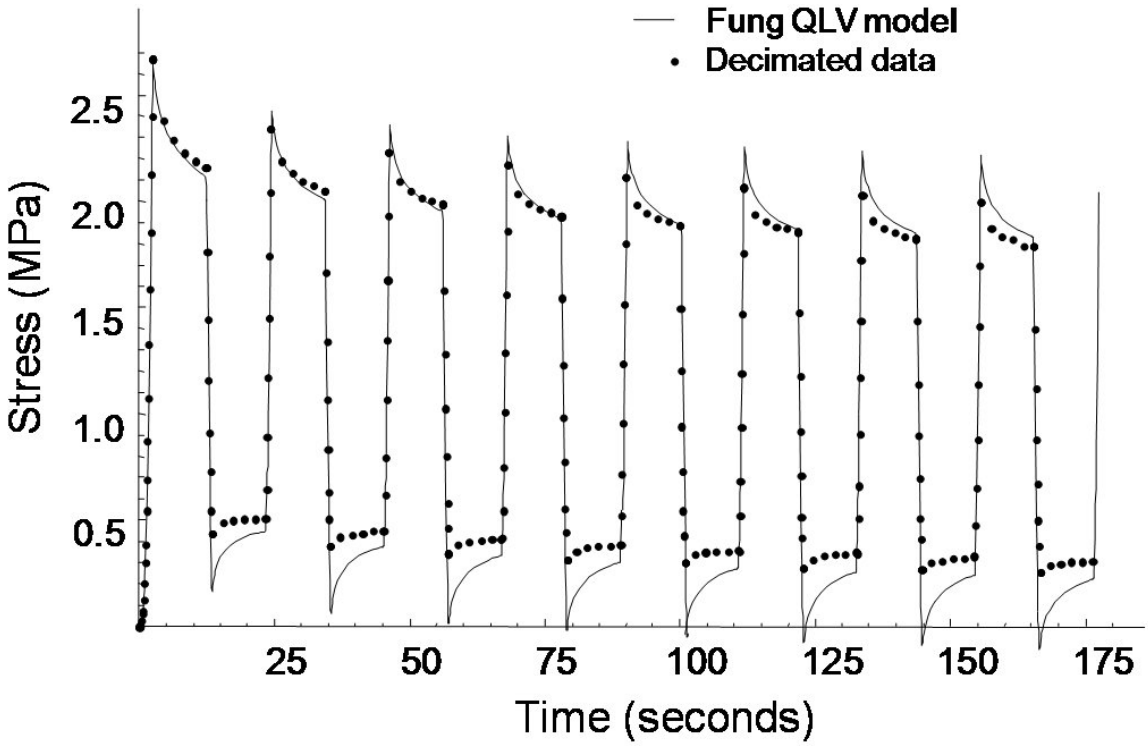

Figure 5.3: The traditional QLV predictions of the specimen stress relaxation for 8 cycles of the ramp-hold-unload-hold testing protocol. The parameters of the model were estimated from a standard stress-relaxation test. The results show that the prediction of the unloading behavior is visibly poorer than the predictions of the loading behavior

The experimental stress response indicates that there are differences in the tissues loading and unloading stress responses. This difference is reflected in the plots; the unloaded tissue appears to have quicker early relaxation, but does not relax as much as when loaded (see figures 5.3 and 5.4). The bidirectional model was formulated to account for this difference in loading and unloading, and

uses two independent parameter sets to represent each behavior. To estimate the two parameter sets of the bidirectional results, we characterized all 8 cycles of the load-hold-unload-hold test protocol. We used a simple load-direction criterion for switching between the two parameter sets.

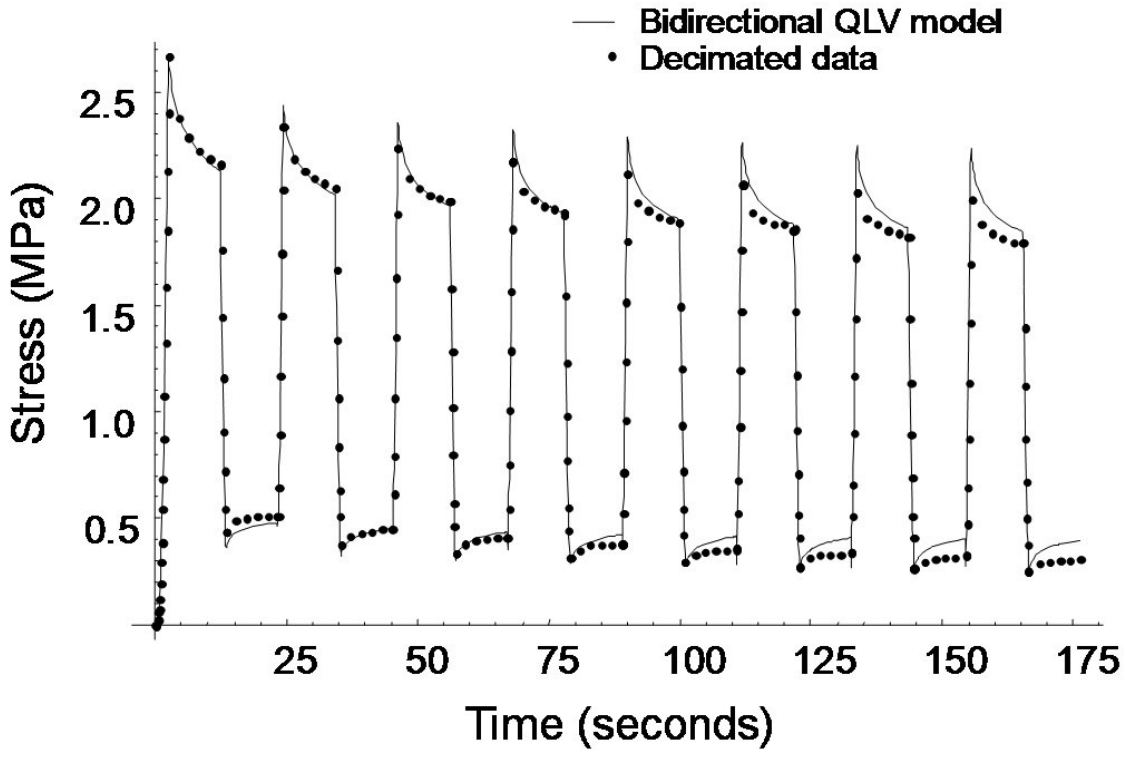

Figure 5.4: A representative theoretical fit of the decimated ramp-hold-unload-hold data for 8 cycles. The bidirectional model was used with independent viscoelastic parameter sets for the loading response and the unloading response

The results show that the bidirectional model performs as well as the Fung model in characterizing the stress-relaxation response of the first loading phase. However, unlike the Fung model, the bidirectional model provides good fits of the unloading stress response.

Figure 5.5 shows that the accuracy of both models deteriorates as the number of cycles increase. However, the error in the traditional model is much larger and increases faster than in the bidirectional model.

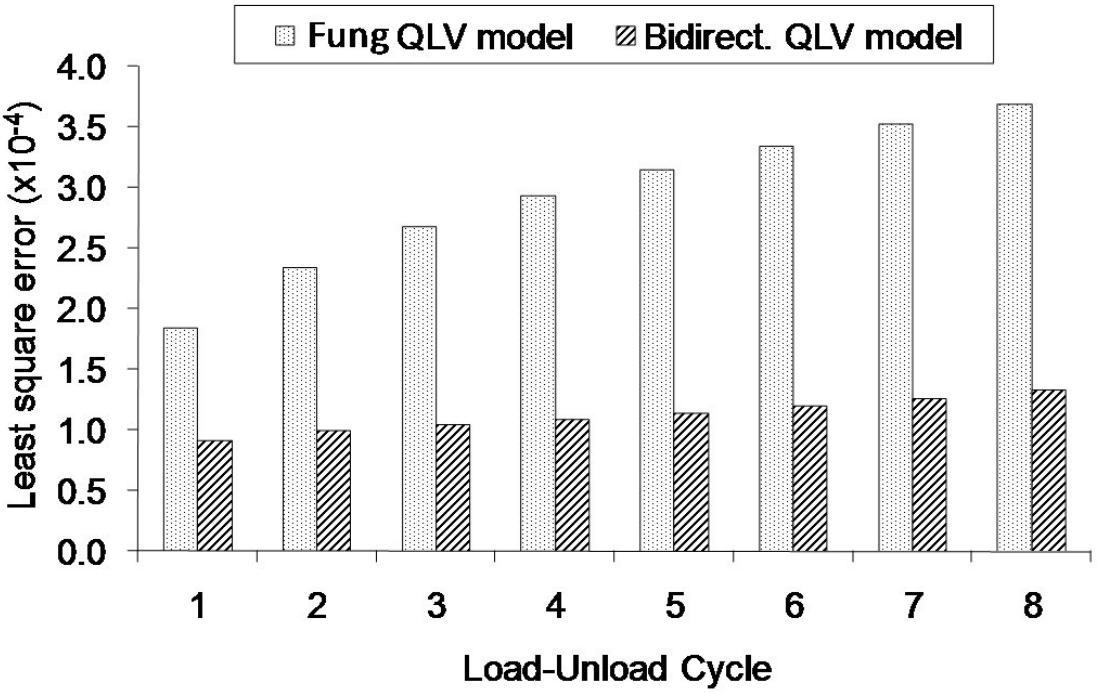

Figure 5.5: Least squares error calculations for the traditional model and the bidirectional model. The error is plotted as a function of number of cycles. The errors of both models increase with increasing cycles, however, the bidirectional model more accurately represents the tissue behavior compared to the traditional QLV model

5.5 Discussion: Bidirectional Model

The work presented in this paper provides insights into the unloading viscoelastic response of Achilles tendon fascicle-groups and presents a modified viscoelastic constitutive model that addresses a long-standing problem of modeling the cyclic load response of soft tissues. Previous studies [73, 56, 59] have shown that the Fung QLV model parameters do not accurately predict the cyclic stress response of soft connective tissues. Our results (figure 5.4) shows that representing the unloading behavior using a separate parameter set, significantly improves theoretical fits of the tissues cyclic stress-strain response. The improved characterization with the two parameter sets strongly suggests differences in the tissues viscoelastic response to loading and unloading.

The results show differences in the Fung model parameters and the unloading parameters of the bidirectional model. Some parameters differ by orders of magnitudes (table 5.1). We found a

statistical difference (students t-test, $n = 6$, $p < 0.05$) only in the C and τ_1 parameters of the Fung model and the C_n and τ_{1n} (i.e. the unloading) parameters of the bidirectional model. We did not expect a statistical difference between the Fung model parameters and the loading parameters of the bidirectional model because both parameter sets are estimated from similar stress-relaxation test. The τ_2 parameters of the traditional model and the τ_{2n} parameter of the bidirectional model were not significantly different, however, during the optimization, we found that large fluctuations in the τ_2 parameter resulted in very small changes in the stress response of the tissue. This suggests that the viscoelastic stress response of the tissue is only weakly governed by the late time constant.

We did not find any significant differences in the loading and unloading nonlinear elastic parameters of the bidirectional model. We simplified our optimizations by estimating the nonlinear elastic parameters of the loading response, and using the same fixed values in the unloading parameter set. Our results are not significantly affected by this simplification. In contrast, the differences in the viscoelastic parameters of the bidirectional model suggest that the unloading behavior is different from the loading behavior. This is also reflected in the plots (see figures 5.3 and 5.4): the unloaded tissue appears to have quicker early relaxation, but does not relax as much as when loaded. Other studies have remarked on the differences in loading and unloading, however, we are not aware of any studies that have provided sufficient details to draw mechanistic conclusions or evolutionary justifications for the phenomenon. The fact that the tissues recovery after unloading is faster than relaxation after loading certainly has physiological relevance. In the case of a runner where injury typically occurs during the loading phase, its role might be to allow the tissues to "reset and prepare quicker for the next stride. By enabling a fairly consistent baseline state at the initiation of loading, the tissue is less prone to overload and potential failure. The different relaxation amounts support a theory of different underlying mechanism in the viscoelastic response of the tissue to loading and unloading. Considering the loading condition essentially forces the tissue into an "un-natural conformation, we expect this boundary condition evokes a different physiological response than unloading, which as an "unforced state may be a reflection of self-governed internal process. From this perspective, characterizing the unloading behavior might be a better method to estimate "natural tissue

properties.

5.6 Conclusions: Bidirectional Model

Our goal was to provide a best-fit of our experimental data to viscoelastic constitutive models for Achilles tendon fascicles. Although the Fung model accurately estimates the peak stresses after loading, it consistently underestimates the tissue stress after unloading. The error may accumulate, and the model fits become increasingly inaccurate with each subsequent cycle (see figure 5.5). We characterized the loading and unloading viscoelastic behavior of the tissue by curve-fitting their stress-strain data and determining regional parameters. We successfully demonstrate that the use of separate parameter sets improves the accuracy of mathematical fits, however, there remain some theoretical limitations; (1) We do not assess the predictive ability of the bidirectional model. A different study where the model parameters are used to predict the stress response of the tissue to a different loading condition is necessary to explore its utility as a predictive model.(2) There is a large computational cost associated with increasing the degrees of freedom. Despite an extensive decimation (maximum of 60 data points), the bidirectional model required approximately 3 hours for full optimization (Dell 32 bit, 2.2GHz). (3) This study does not explore the underlying mechanism of action of the tissues responses. As such, it is likely that the results are valid only for connective tissues subject to tensile loads.

In comparing the Fung model to our new bidirectional QLV model, we use the exact same data processing and analysis procedures. Thus, the improvements shown in this study are due to the bidirectional models ability to account for the unloading behavior. Our results show that there are significant differences in the viscoelastic parameters characterizing the tissues responses to loading and unloading. We also show that the bidirectional modeling approach provides significantly better the characterizations of the experimental cyclic test profile than the Fung model. This indicates that the model may be useful for the formulation of computational models of tissue structures in complex load/unload conditions.

Chapter 6: A HETEROGENEOUS FINITE ELEMENT ANALYSIS OF LOCAL STRESSES IN THE ACHILLES TENDON FASCICLES

6.1 Summary

In this study, a 3-D multi-domain finite element(FE) model is used to investigate local stress distributions within small (n $<$ 20) groups of Achilles tendon fascicles. Existing soft tissue models generally assume homogeneous material properties for all sub-macroscopic tissue components. However, a microscopic inspection of Achilles tendon fascicles reveal a soft reticular membrane (i.e. endotenon) surrounding individual fascicles. We model individual fascicles as multi-domain composites of the fascicle material and the surrounding endotenon. Groups of these heterogeneous fascicles are subjected to simulated uniaxial and shear tests. Our results show lower stress values in the heterogeneous model as the relative difference in moduli of the fascicle and endotenon material increases. The results are then compared to a homogeneous model of comparable macro-structure and we show that the stress distributions within the fascicles are lower in the heterogeneous model. There are significant obstacles to an experimental validation of these results, however, they suggest a direct relationship between the underlying microstructure of fascicles and their local stress distributions.

6.2 Introduction: F-E Analysis

Tendons and ligaments have a complex collagen microstructure that is likely optimized for the transfer of tensile loads. The aggregate collagen molecules are organized in a successive hierarchy of fibrils, fibers, fiber bundles, and fascicles [2, 77]. In the Achilles tendon, the fascicles are long and generally parallel. They are surrounded by a sheath of reticular membrane(i.e. endotenon) which serves multiple functions: to promote relative movement (i.e. sliding) of adjacent fascicles; as a vascularized and innervated layer of connective tissue.

Finite element (FE) models have been used to investigate the deformation behavior of many different soft tissues [78, 79, 80, 81]. However, these analyses have utilized continuum based consti-

tutive formulations of the material, and are therefore inadequate for analysis of the load contribution of the different sub-structural components of the tissue. We are not aware of any FE studies that have analyzed the stress distribution within fascicle and non-fascicle structures in a tendon. A major obstacle has been the challenge of generating a robust, high quality multi-domain 3-D mesh for a finite element analysis. Commercially available multi-domain meshing algorithms(e.g. Hypermesh^{TM}, Simpleware^{TM}) are expensive and typically generate meshes that contain numerous thin elements ('slivers'), jagged surfaces and other undesirable artifacts that prohibit subsequent FE analysis. The FE mesh used in this study is generated from a segmented volumetric representation of the fascicle and surrounding endotenon. A fully automated multi-domain mesh generation system previously developed in our lab is used to create the FE mesh. The system uses a combination of MATLAB^{TM} programs and open-source CGAL mesh generation software (cgal.org). It significantly improves the mesh quality using new algorithms for robust boundary preserving sliver removal and multi-domain surface revoxelization.

In this study, a 3-D multi-domain finite element(FE) model is used to investigate the local stress distributions within small ($n < 20$) groups of Achilles tendon fascicles. The specimen is modeled as a heterogeneous composite of the fascicle material and surrounding endotenon, directly incorporating the tissue structural information into our simulations. We vary the relative moduli values of the fascicle and endotenon material from equal (i.e. homogeneous material) values, to different degrees of heterogeneity. This allows us to investigate the effect of changes in the heterogeneous material properties on the overall stress response of the tissue. Our results show that there is a reduction in the overall stress distribution values in the heterogeneous model indicating the physiological microstructural organization is likely optimal for reducing the stresses within the tendon.

6.3 Methods and Materials

6.3.1 Creating the volumetric model

To create the model, an image manipulation program(GIMP 2.6.7, GNU/Linux) was used to trace a 508x462 pixel region of 16 closely connected, distinct fascicles of various cross sectional shapes and areas from a high resolution cross-sectional image of a human Achilles tendon. Exact measure-

ment of the endotenon thickness was not possible, so the thickness of the surrounding endotenon was approximated by shading the regions between the individual fascicles. The two dimensional trace was imported into MATLAB®, and processed to generate an indexed, multi-domain dataset of the fascicles and the surrounding endotenon membrane. A simple volumetric model was then created by stacking the resulting 2-D images along the axis perpendicular to the image plane. A final model, a 3-D volumetric array (508x482x40) is generated. The key steps are highlighted in figure 6.1.

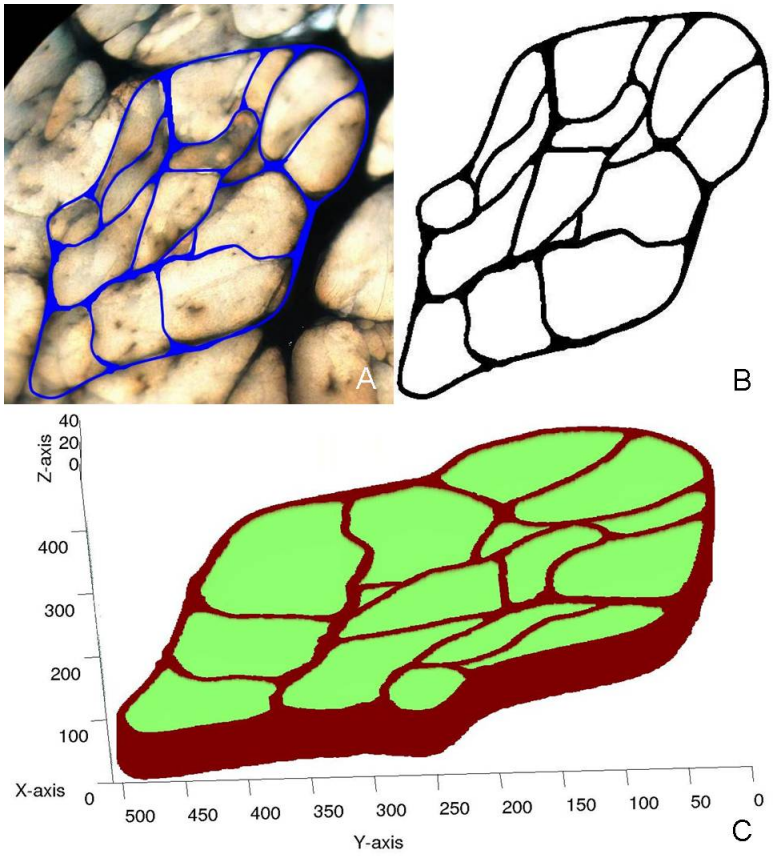

Figure 6.1: (A) An intimately connected sub-group of 16 fascicles is traced from the original high resolution cross section of a human Achilles tendon (B) the trace image is converted to an indexed, two domain dataset in MATLAB® (C) An volumetric dataset is created by stacking the 2-D image along the Z-axis

6.3.2 Model Assumptions

As described, the volumetric dataset of the model was created by stacking 2-D images along the perpendicular axis. This approach enforces an assumption of a parallel organization of the individual

fascicles. However, as discussed by Cummins et al. [39], there is a slight spiraling, or "twist" of the tendon fascicles as the tendon fibers of the gastrocnemius rotate around the fibers originating from the soleus. Another assumption of this model is the representation of fascicles as distinct and single units. This is likely a limitation of the available visualization as we are not at this time, capable of exactly resolving intimately connected fascicles.

6.3.3 Generating a 3-D finite element mesh

A high quality multi-domain unstructured tetrahedral mesh was created using a mesh generation algorithm developed using MATLAB^{TM} and the CGAL open source software libraries [82]. The mesh generation algorithm, developed by Doehring, is fully automated and capable of multi-domain meshing directly from indexed or segmented voxel images. The mesh was controlled for minimum surface face angle, maximum surface triangle size, geometry surface-fit tolerance, element "quality" and maximum element volume. The mesh quality was calculated using a standard formulation for tetrahedral meshes described by Persson, i.e. as a ratio of the radii of the inscribed and circumscribed spheres [83]. A robust, boundary preserving sliver removal algorithm was used to remove thin, low quality elements and forestall instability in the subsequent finite element(FE) analysis. A convergence test was performed to optimize the number of elements. For a surface fit tolerance of a single pixel, we generated a mesh of 38,272 nodes and 187858 elements(figure 6.2).

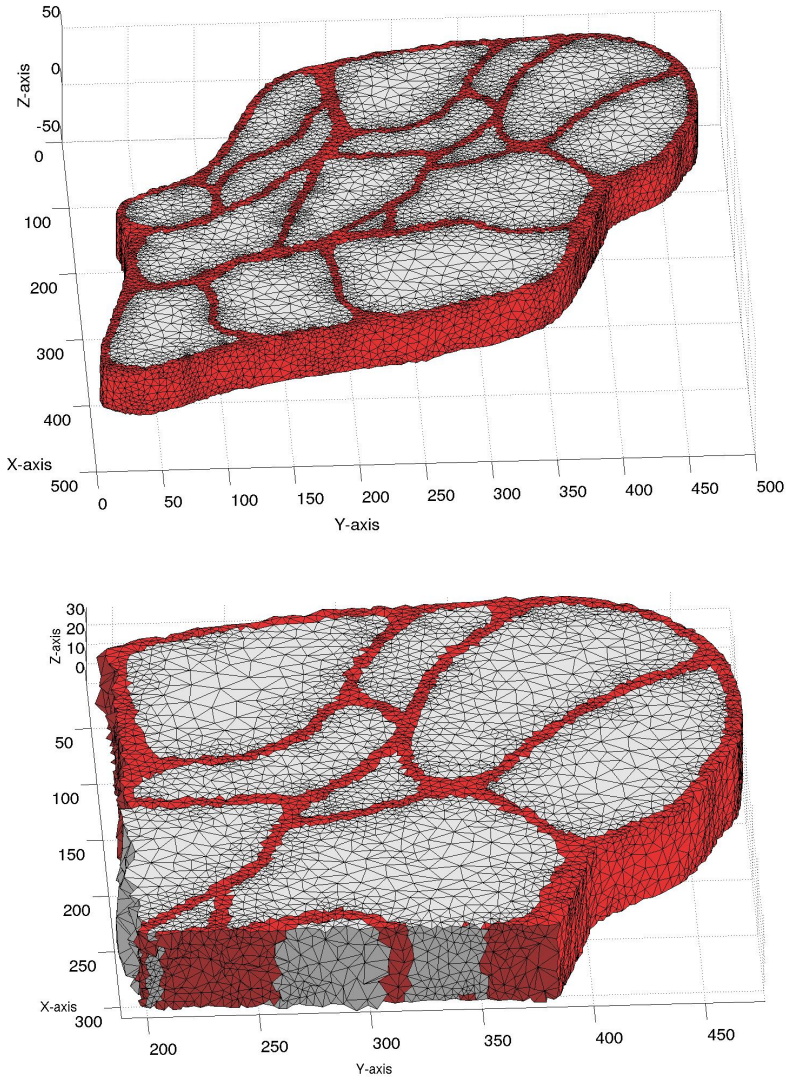

Figure 6.2: (A) A section of the unstructured mesh of 38,272 nodes and 187,858 tetrahedral elements. (B) The elements show a regular size gradient on the surface and through the the volume.

6.3.4 Finite element analysis

We simulated a uniaxial tensile test and a shear test in TOCHNOG (tochnog.sourceforge.net), an open source finite element program. The analysis was executed on an 8-dual core AMD Opteron™ computer running Ubuntu(Linux version 2.6.29-19-generic) operating system. Available options in TOCHNOG were used to reduce the problem complexity: Inertia terms were not included in the analysis and a single integration point, in the geometric middle, was assigned for each tetrahedral

element.

The fascicles were modeled as a linear solid material using a Young's modulus(86.1 MPa) and Poisson's ratio(0.4) from the literature [84]. The modulus value was also consistent with the values we found in the study presented in Chapter 4 (see table 4.1). The endotenon material properties were defined as a percentage of the fascicle modulus. Four different analysis were performed. In the first, the endotenon modulus was defined as 100% of the fascicle modulus, essentially modeling the entire volume as a homogeneous material. In subsequent analysis, the endotenon modulus was defined as 50%, 10% and 1% of the fascicle's Young's modulus.

Uniaxial tensile test

The uniaxial tensile test was simulated in the FE analysis by uniformly displacing the top surface nodes of the model axially in the Z-direction. The bottom surface nodes were constrained in the Z-direction. To prevent rigid body rotations, two randomly selected bottom nodes, located "far" from each other were also constrained in the X- and Y- directions.

Shear test

The shear test was also simulated as a displacement controlled test. The bottom nodes were completely constrained in the X-, Y- and Z-directions and the top surface nodes were collectively displaced in the X-direction. We applied a total displacement of 6mm using small 3 timesteps at intervals of 1 millisecond.

6.4 Results

Figure 6.3 is a color map of node displacements confirming correct application of the uniaxial tensile boundary conditions. The bottom nodes are fixed in the loading direction and show no displacements in the axial loading direction. The displacements are uniformly applied on the top nodes, and as expected, the node deformations show a uniform, stratified gradient through the model volume.

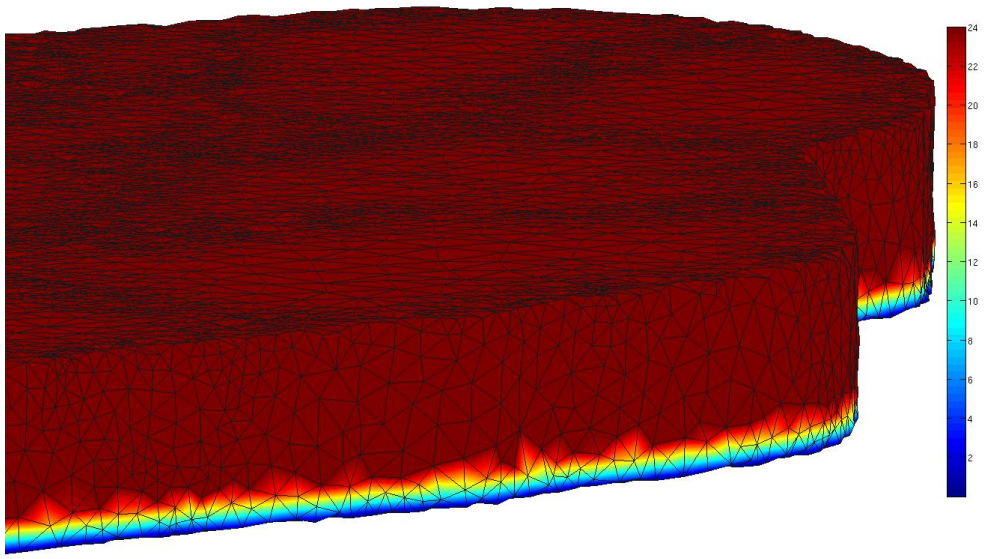

Figure 6.3: Color map of nodal displacements for uniaxial tension test. The bottom nodes (blue) are fixed and the axial displacement is applied to the top nodes

Figure 6.4 is a scaled color map of the von mises stress results from a representative FE analysis on a model with an endotenon modulus equal to 50% the fascicle modulus. It is clear the regions within the fascicles have significantly higher stresses than the surrounding endotenon material. This result was consistent for all the fascicle models with softer endotenon moduli. In the case of equal modulus for the fascicle and endotenon (i.e. a homogeneous material), as expected, there was no difference in the relative stress values.

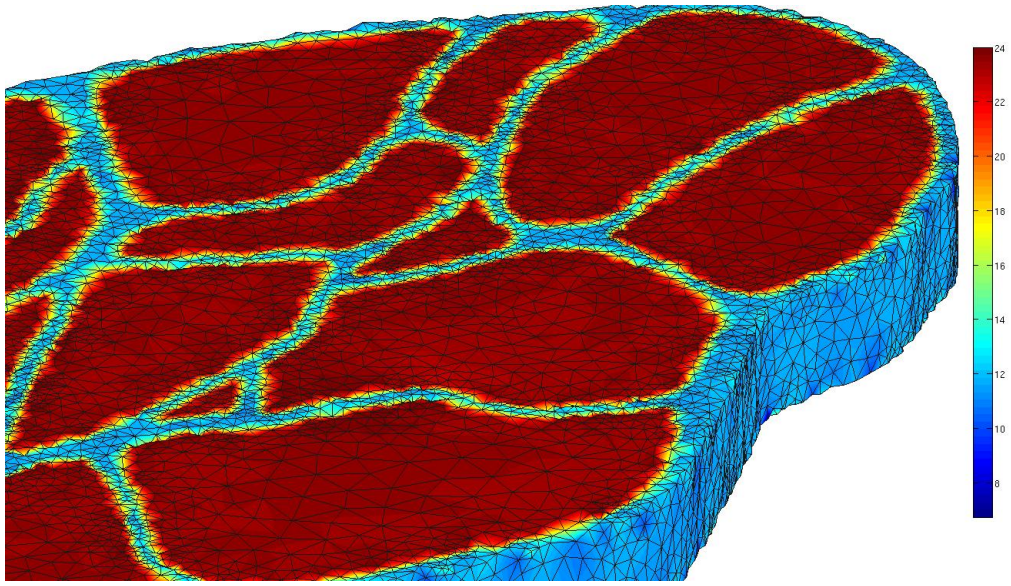

Figure 6.4: A color map of the Von-Mises stress distribution for an endotenon modulus of half the fascicle modulus. As expected, the fascicle stresses are much higher than the endotenon stresses.

In figure 6.5, we present combined bar-plots of the Von-Mises equivalent stress, the mean, and the median stresses from the uniaxial tensile tests. The plots are grouped for the different endotenon moduli (expressed as as percentage of fascicle modulus), and sub categorized into the "overall," "fascicle," and "endotenon" stresses. The overall is a simple average over the entire cross-section of the specimen. The fascicle and endotenon regions refer specifically to those regions as referenced by the moduli values defined within the region.

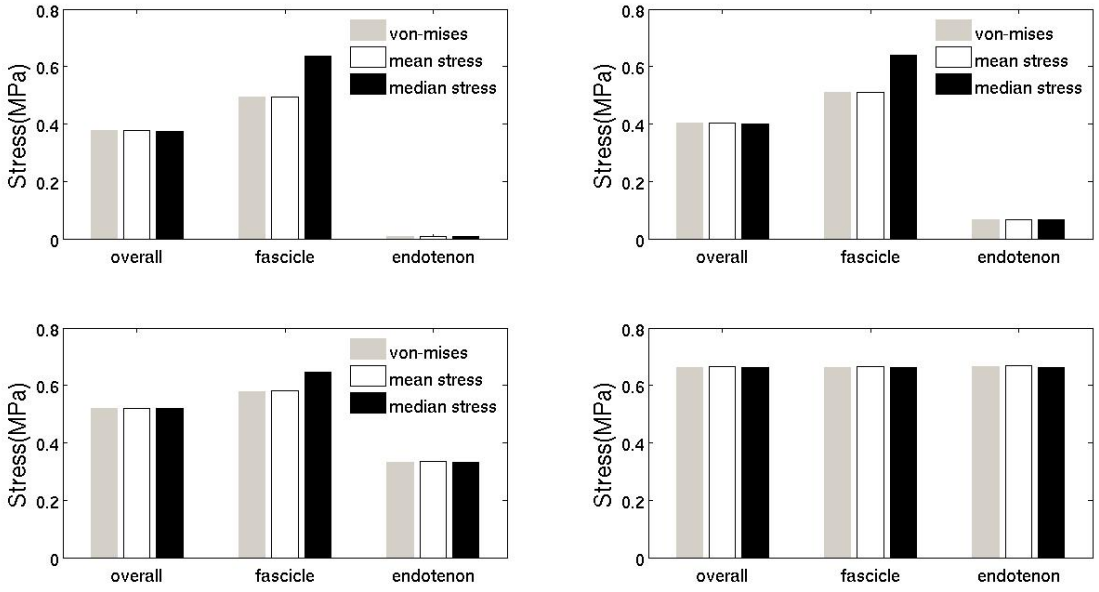

Figure 6.5: Bar plots for the overall specimen, the fascicle and the endotenon. The plotted stress distributions are for four different endotenon moduli values. The endotenon modulus is expressed as a percent of the fascicle modulus. From left to right and top to bottom, they are 1%, 10%, 50% and 100% respectively.

Attempts to generate similar plots for the shear tests results were unsuccesfull. Despite confirming proper application of the displacement boundary conditions, i.e. top surface nodes were displaced in the Z-direction, it was not possible to obtain consistent results from our stress analysis. Figure 6.6 is a bar-plot of the Von-Mises, mean stress and median stress for the shear stress analysis of the case of an endotenon modulus equal to 100% of the fascicle modulus.

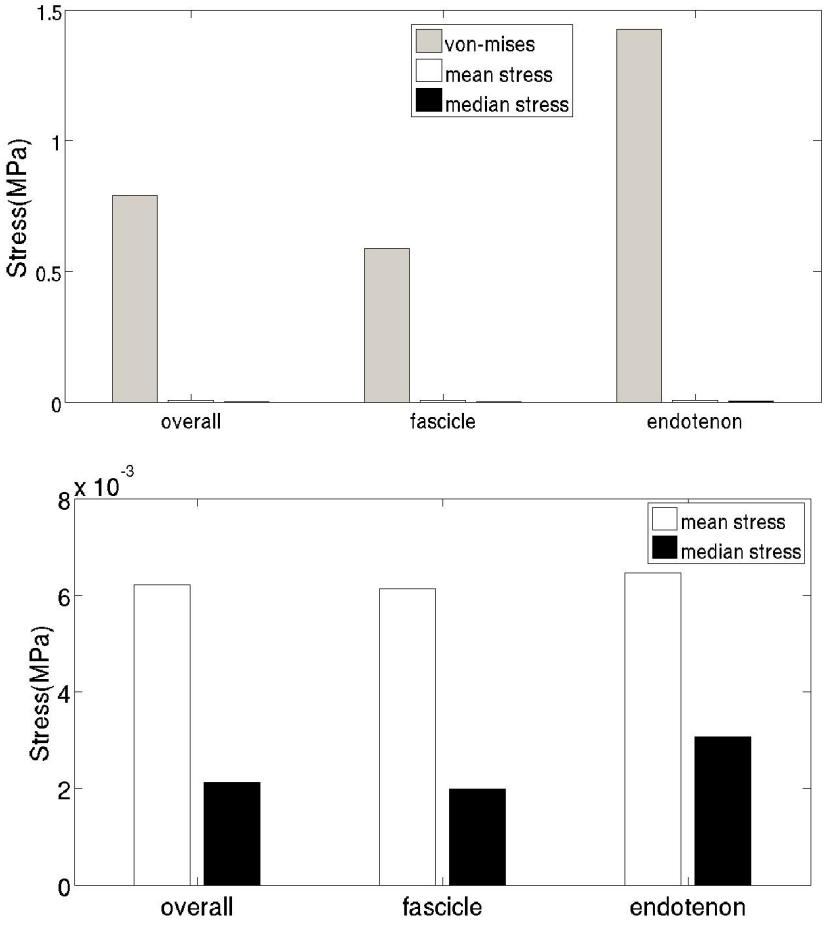

Figure 6.6: Von-Mises, mean shear stress and median shear stress for the case with an endotenon modulus of 100% of the fascicle modulus. The Von-Mises plots would indicate that the endotenon stresses are higher than the overall and fascicle stresses. However, the low mean and median stresses indicate the specimen was likely not loaded to levels necessary for an accurate analysis.

6.5 Discussion: F-E Analysis

The deformation patterns confirm correct application of the boundary conditions. For the uniaxial tensile case, the constrained bottom nodes show zero deformation in the loading direction, and the top-surface nodes undergo the maximum deformations in the axial, Z-direction. All the specimens are loaded to the exact same displacement level. The implication for our results is that we expect the maximum stresses of the model to be proportional to the relative stiffness of the fascicle and endotenon material. The plots of Figure 6.4 show correctly that as we soften the endotenon modulus (from 100% of the fascicle modulus, to 1% of the fascicle modulus), the maximum stresses experienced

by the overall model decreases.

To understand how the heterogeneous structure contributes to the overall tissue response, we analyze the fascicle and endotenon stresses separately and relate them to the overall specimen stresses. We use the Von-Mises stress and the mean and median stresses in the principal loading direction as indicators of stress behavior. The Von-Mises stress is usefully for confirming correct behavior of the FE model. Since we apply purely uniaxial loads, there are very little off-axial load contributions to the Von-Mises equivalent stress, and we expect the Von-Mises stresses should coincide with the mean stresses in the loading direction.

In Figure 6.5, the results show a decreasing overall specimen and fascicle stresses, with softening of the endotenon modulus. Physiological relevant moduli can be approximated between 10% and 50%, and we show quantitatively that at these relative values, the overall stresses and the fascicle stresses decreases. We confirm that at equal material properties (i.e. endotenon modulus is 100% of fascicle modulus), the overall, fascicle and endotenon stress behaviors are identical. Essentially, by disregarding the heterogeneous structure, the specimen behaves as an isotropic material. These results provide a biomechanical rationale of the experimental observation that most load supporting aggregate structures are typically surrounded by a softer reticular membrane.

We also present the results from a simulated shear test analysis. We were not able to obtain consistent results. We analyzed the 1%, 5%, 10%, 30%, 80% and a 100%. In a seemingly random pattern, at 1%, as expected, the fascicle shear stress was higher than the endotenon, at 5%, 10% and 50%, the fascicle stresses were negative, and the endotenon positive. At 80%, the endotenon stresses were higher, and at 100%(see figure 6.6), the mean stresses were relatively equal. We maintained the same boundary conditions in all cases, as that was the only way to independently assess the effect of the heterogeneous structure. These results strongly indicate that our testing protocol for the shear test was not accurate. In future analysis, it may be necessary to increase the applied displacement, increase the iterations of our solutions or reduce the size of our time steps.

There are a number of limitations to direct application of these results. Although general trends can usually be inferred from FE analysis, these numerical methods are prone to local stress concen-

trations and require extensive convergence studies. In addition to carefully setting up our FE mesh and analysis, we manage local stress concentrations by reporting mean values of stress as opposed to absolute maximums and minimums. It would be informative to compare our results to a load controlled test. Unlike a displacement controlled loading, the results should directly indicate the different loading on the fascicle with changing endotenon moduli

Despite these limitations, this study has successfully demonstrated that the heterogeneous structure has a direct effect on the stress distribution on fascicles. Our results show that representing the endotenon as a softer material, lowers the overall and fascicle stresses. Current models that model the tendon material as having homogeneous properties may be reporting higher fascicle stresses than the natural stress state of the tissues.

6.6 Conclusions: F-E Analysis

In this study, we model individual fascicles as multi-domain composites of the fascicle material and the surrounding endotenon. We demonstrate that the heterogeneous structure and material properties directly contribute to the overall stress response of the specimen. Interestingly, our results also show lower stress values within the fascicles of the heterogeneous model as the relative difference in moduli of the fascicle and endotenon material increases. The results of this study suggest a direct relationship between the underlying microstructure of fascicles and their local stress distributions. This is particularly important and applicable to fascicle and fiber scale computational models of soft collagenous tissues.

Chapter 7: Conclusions and Future Recommendations

7.1 Review of Overall Goals

The origins of this research project were based on the paucity of information in the literature concerning the load distribution and mechanical properties of the sub-macroscopic components of connective tissues. The human Achilles tendon is a optimal study subject for a number of reasons. Clinically, the Achilles tendon is the most frequently ruptured tendon in the human body and accounts for 40% of all operated tendon ruptures. There is evidence of an increasing incidence of Achilles tendon rupture, however, hitherto, rupture has been sudden and catastrophic with little or no discernible clinical indications of the imminent rupture. The standard computational biomechanics approach to understanding failure of soft tissues is the development of analytical and structural models of the tissue's load response. Existing studies of the Achilles tendon have generally focused on the tissue's macroscopic behavior. However, despite best efforts, these studies remain unable to provide accurate and reproducible information on the biomechanical properties and loading behavior of the tendon's sub-macroscopic scale components. This knowledge is critical to understand and develop surgical or tissue engineered interventions to the problem of injury, particularly sub-failure injury.

In this thesis, we define three research areas, each with specific objectives. In the first, we determine the linear and nonlinear biomechanical properties of individual fascicles as well as the inter-fascicle load distribution within aggregate groups. In the second, we address the poor characterization of the cyclic load response of tissues by existing viscoelastic models. Specifically, we investigate the differences in the viscoelastic stress response of Achilles tendon fascicles to loading and unloading. In the third area of study, we use a finite element model to investigate the local stress distribution within small groups of Achilles tendon fascicles. By utilizing a multi-domain mesh generation system, we are able to directly incorporate the heterogeneous structural information directly into our simulations.

7.2 General Review of Results

In the fascicle scale loading and failure study, we find the modulus of the strongest fascicle was on average, 3.5 times that of the intact specimens. Some individual fascicles were even stronger, up to 5 times the intact specimen. These consistently higher moduli values of the strongest fascicle, as well as the observed load distribution, indicate that the overall response of the tendon may be dominated by a subset of "strongest fascicles".

During loading, the fascicles initially rotated into the direction of loading. These rotations could be the result of forcing the specimen out of its optimal in-situ alignment (clamping effects, etc.), but they also could be present in-vivo. Small loads are carried during rotation, even when the fibers are not tensed. We made every effort to select the gage length after large rotations were complete and the specimen was carrying load.

The experimental stress response plots of the bidirectional viscoelastic study indicates differences in the tissues loading and unloading stress responses. The unloaded tissue appears to have a quicker early relaxation, but does not relax as much as when loaded. The bidirectional model was formulated to account for this difference in loading and unloading, and uses two independent parameter sets to represent each behavior. The results show the parameters of the Fung Quasi-Linear Viscoelastic (QLV) model and the loading parameters of the bidirectional model are not significantly different. Both parameter sets are estimated using similar stress-relaxation test. However, there is a significant difference (students t-test, $n = 6$, $p < 0.05$) between the parameters of the Fung model and the unloading parameters of the bidirectional model. The estimated parameters were used to predict the stress response to all 8 cycles of the load-hold-unload-hold protocol. The Fung model accurately predicted the stress relaxation response of the first load phase. By the first unloading phase, it is clear that the Fung model provides a poor fit of the unloading data. This error compounds, and subsequent loading and unloading cycles are also poorly fit. The bidirectional model performs as well as the Fung model in characterizing the stress-relaxation response of the first loading phase. However, unlike the Fung model, the bidirectional model provides good fits of the unloading stress response.

In the finite element microstructural study, the results show the regions within the fascicles have significantly higher stresses than the surrounding endotenon material. This result was consistent for all the fascicle models with softer endotenon moduli. In the case of equal modulus for the fascicle and endotenon (i.e. a homogeneous material), as expected, there was no difference in the relative stress values within the fascicle material and the endotenon. We also find that surrounding the relatively higher modulus fascicle with a lower modulus endotenon contributed to lowering the overall stresses across the cross section of our model, as well as within the fascicle material.

7.3 Important Findings

1. **The overall load response of the tendon may be dominated by a subset of "strongest" fascicles**

   We find that that a few fascicles appear to support significantly higher loads than other fascicles. Normalizing for differences in cross sectional area, the modulus of this group of strongest fascicles is on average, 3.5 times the modulus of the other fascicles. This results has implications in our understanding of Achilles tendon rupture, and suggests a "critical" subgroup of fascicles.

2. **Non-affine deformations may contribute to low clinical rupture loads of the Achilles tendon**

   An unresolved paradox of the Achilles tendon is that clinical reports suggest much lower rupture load levels than biomechanical failure load levels indicate. By directly measuring the deformation of individual fascicles loaded within aggregate groups, we demonstrate the presence of significant non-affine(rotations and fascicle-to-fascicle sliding) deformations. The stresses generated from these non-affine deformations are not typically accounted for in most failure studies, and it is also likely that meticulous specimen preparation and loading may preclude this behavior, resulting in higher experimental failure loads.

3. **Achilles tendon fascicles have a significantly different loading and unloading viscoelastic stress response**

It is usually assumed that tissues exhibit symmetric, mirrored loading and unloading behaviors. Model parameters estimated from loading tests, and used to characterize cyclic behavior usually represent peak stresses with high accuracy, but consistently underestimate the valley stresses. We show significant improvements in characterization of Achilles tendon fascicles' viscoelastic cyclic stress-strain response by representing the unloading behavior with a separate, uniquely estimated parameter set. The improved characterization strongly suggests differences in the underlying governing mechanisms of loading and unloading.

7.4 Contributions to field of Biomechanics

The results presented in this work demonstrate a successful characterization of the fascicle scale stress response of the Achilles tendon. We introduce a number of experimental techniques for determining the material properties of individual fascicles and aggregate groups of fascicles. We also introduce a novel loading protocol capable of exciting the viscoelastic response of a tissue to loading and unloading. We successfully demonstrate the use of advance digital image correlation algorithms to directly measure local specimen deformation. This non-contact, yet highly accurate deformation measurement technique has not previously been available in the field. We present a bidirectional constitutive model that demonstrates significantly improved characterization of Achilles tendon fascicle stress responses to cyclic loads. Finally, using a simple 3-D FE model, we are able to qualitatively demonstrate the effect of heterogeneous mechanical properties on the local fascicle stresses.

7.5 Limitations

In the course of work, there were a number of experimental and analytical limitations that are detailed in the body of this thesis. For completeness, we revisit a number of those limitations in the study conclusions.

In the fascicle scale loading and failure study, elliptically polarized light is used to image the Achilles tendon fascicles. It is well established that the collagenous tissues have a natural birefringence and imaging using polarized light offers significant improvements in visualization of internal

structures. We note that despite these improvements, we were not able to perfectly resolve intimately connected fascicles. Our results show that the experimental load bearing capacity of single fascicles is significantly higher than the load bearing capacity of individual fascicles analyzed within a group. However, our results for single fascicles may be unduly influenced by tightly cross-linked multi fascicles. This will significantly increase estimates of the maximum load supported by single fascicles. To control for this limitation, we verify all experiment using simultaneously acquired video data. We visually inspect the data for abnormal behavior such as excessive rotations, or sudden fluctuations in carried loads of the tissue.

Despite the established evidence of interwoven fiber arrangements of soft collagenous tissues, our F-E computational model remains based on the parallel fiber model of tendons and ligaments. Our model was used to investigate the effects of the heterogeneous microstructure on the local stresses in fascicles. The parallel fiber simplification was helpful in reducing the order of complexity of the overall problem, but may also limit application of our results. Our results may only have qualitative relevance, indicating that the heterogeneity of the microstructure does in fact affect the local stresses in the fascicle. We find that as the modulus of the surrounding endotenon reduces, there is a corresponding reduction in the stress levels in the fascicle. Due to the approximate parallel model used in this study, the results are likely only directly valid for connective tissues in very narrow ranges of tensile loading.

7.6 Future Directions

This research has produced valuable new data regarding the fascicle scale loading behavior of the Achilles tendon. Each of the specific aims from Section 2.2 was achieved. Recommended future directions of this study are detailed as follows.

7.6.1 Mathematical modeling- Meshless methods

In early stages of this work, we recognized that the complex stress response of soft collagenous tissues necessitated a paradigm shift from the standard FE approach used for engineering materials to a flexible numerical analysis technique. We explored meshless methods as a possible substitute

technique. Unlike a FE analysis, a meshless analysis does not discretize the problem domain using meshes of predefined connectivity, but instead, use only nodes in the domain and on the boundary to continuously update localized shape functions to approximate field variables. The advantage of such a technique for soft tissues is that it avoids instabilities and convergence issues associated with FE mesh distortions. The lack of a mesh also enables deformations that violate the continuum assumptions. Therefore fascicle separations, and other potentially non-affine deformations can be modeled. Despite the literature on the use of meshless methods for force feedback modeling of soft tissues and organs in virtual reality training simulators, it was impossible at this stage to successfully incorporate the technique at the modeling scales of this work. Future studies on the fascicle and sub-fascicle scale modeling of soft tissues will benefit greatly from implementation of meshless techniques

7.6.2 Modeling Contact

An important direction is the incorporation of a contact analysis in existing tissue models. Contact refers to a physiological based nodal connection between adjacent substructures in a model. Contact analysis creates a highly nonlinear problem and at the time of this work, we are not aware of any groups that are exploring a contact based analysis of soft collagenous tissues. Despite our best efforts, our efforts were limited by inadequate computational tools. This level of accuracy will be essential for calculating localized stress distributions, in and around the tissue.

7.6.3 Small Scale Experimental Testing

The data used in this research were obtained using testing system that was developed for group fascicle scale tests. Extensive work, not included in this thesis has already been done to develop a single-fascicle scale testing system. Testing systems such as these are necessary for complex experimental loading protocols in torsion, shear, and buckling analysis. Results of these analyses are essential to completely characterize tissue behavior and material properties at single fascicle, and smaller scales.

7.7 Concluding Remarks

This thesis presents results from a novel, fascicle scale experimental and computational approach to investigating the structure-function relationship of the Achilles tendon. We successfully accomplished our goals of (1) performing fascicle-scale experiments, (2) analyzing tensile data using novel viscoelastic models and (3) developing a 3-D computational model of tendons that begin to account for fiber to fiber-sliding and other non-affine deformations. Many insights into the fascicle scale behavior of the Achilles tendon have been obtained. We find that the overall load response of the Achilles tendon may be dominated by a subset of strongest fascicles; that non-affine deformations may contribute to low clinically reported rupture loads of the tendon and the Achilles tendon fascicles have a significantly different loading and unloading viscoelastic stress response. These findings are particularly important for the formulation of microstructural models attempting to predict cell-matrix stresses and inform on sub-failure injury.

Collagenous tissues like the Achilles tendon have a highly complex and intricate microstructure. A vast amount of information has been gleaned from existing macroscopic deformation studies. However, we believe that the clinical problems of injury and repair –our ultimate motivation, can only be addressed through an understanding of the tissue's sub-macroscopic mechanical properties and deformation behavior. By characterizing the fascicle scale behavior of the Achilles tendon, we provide a quantitative basis for assessing the sub-macroscopic scale performance of other microstructural models.

Further developments, particularly in the synthesis of sub-macroscopic experimental data and computational modeling techniques, are essential for an improved understanding, effective repair and ultimately, functional tissue engineered replacements of diseased and injured tissues.

Bibliography

[1] Mitsuhiro Aoki, Naoshi Ogiwara, Takayuki Ohta, and Yuki Nabeta. Early Active Motion and Weightbearing After Cross-Stitch Achilles Tendon Repair. *The American Journal of Sports Medicine*, 26(6):794–800, 1998.

[2] J. Kastelic, A. Galeski, and E. Baer. The multicomposite structure of tendon. *Connective Tissue Research*, 6(1):11–23, 1978.

[3] A. Pare. Workes (translated by t. johnstone). *London*, page 285, 1665.

[4] L. Klenerman. The history of the achilles tendon and its rupture. In N. Maffulli and C. Almekinders, editors, *The Achilles Tendon*. Springer, 2007.

[5] L. Jozsa, M. Kvist, B.J. Balint, A. Reffy, M. Jarvinen, M. Lehto, and M. Barzo. The role of recreational sport activity in Achilles tendon rupture. *The American Journal of Sports Medicine*, 17(3):338–343, 1989.

[6] Anders Moller, Mats Astrom, and Nils E Westlin. Increasing incidence of achilles tendon rupture. *Acta Orthopaedica*, 67(5):479–481, 1996.

[7] Juhana Leppilahti, Jaakko Puranen, and Sakari Orava. Incidence of achilles tendon rupture. *Acta Orthopaedica*, 67(3):277–279, 1996.

[8] GW. Hess. Achilles tendon rupture. *Foot and Ankle Specialist*, 3(1):29–32, 2010.

[9] Anthony A. Schepsis, Hugh Jones, and Andrew L. Haas. Achilles Tendon Disorders in Athletes. *The American Journal of Sports Medicine*, 30(2):287–305, 2002.

[10] Nicola Maffulli and Adam Ajis. Management of Chronic Ruptures of the Achilles Tendon. *J Bone Joint Surg Am*, 90(6):1348–1360, 2008.

[11] G. Puddu, E. Ippolito, and F. Postacchini. A classification of Achilles tendon disease. *The American Journal of Sports Medicine*, 4(4):145–150, 1976.

[12] Mika Paavola, Pekka Kannus, Tero A.H. Jarvinen, Karim Khan, Laszlo Jzsa, and Markku Jarvinen. Achilles Tendinopathy. *J Bone Joint Surg Am*, 84(11):2062–2076, 2002.

[13] Nicola Maffulli. Current concepts in the management of subcutaneous tears of the achilles tendon. *Bulletin: Hospital for Joint Diseases*, 57(3):152 – 158, 1998.

[14] T E O Schubert, C Weidler, K Lerch, F Hofstdter, and R H Straub. Achilles tendinosis is associated with sprouting of substance P positive nerve fibres. *Annals of the Rheumatic Diseases*, 64(7):1083–1086, 2005.

[15] V. So and H. Pollard. Management of achilles tendon disorders: a case review. *Australas. Chiropr. Osteopathy.*, 6(2):58–62, 1997.

[16] H. Alfredson and R. Lorentzon. Chronic achilles tendinosis: recommendations for treatment and prevention. *Sports Med*, 29:135–146, 2000.

[17] L.G. Jozsa and P. Kannus. *Human Tendons: Anatomy, Physiology, and Pathology*. Human Kinetics, 1997.

[18] S. Curvin and W.D. Stanish. *Tendinitis: Its etiology and treatment*. Lexington: Collamore Press, DC Heath, 1984.

[19] R.P. Welsh and J. Clodman. Clinical survey of achilles tendinitis in athletes. *Can Med Assoc J*, 122:193 – 195, 1980.

[20] S.L. James, B.T. Bates, and L.R. Osternig. Injuries to runners. *Am J Sports Med*, 6(2):40 – 50, 1978.

[21] D.M. Brody. Running injuries: Prevention and management. *Clin Symp*, 39:1 – 36, 1987.

[22] D.B. Clement, J.E. Taunton, and G.W. Smart. Achilles tendinitis and peritendinitis: Etiology and treatment. *Am J Sports Med*, 12:179 – 184, 1984.

[23] P.A. Houglum. Soft tissue healing and its impact on rehabilitation. *J Sport Rehabil*, 1:19–39, 1992.

[24] J.B. Rogoff. *Manipulation, Traction and Massage*, volume 2nd ed. Baltimore: Williams and Williams, 1989.

[25] D.W. Rivenburgh. Physical modalities in the treatment of tendon injuries. *Clin Sports Med*, 11:645 – 659, 1992.

[26] M. Moller, T. Movin, H. Granhed, K. Lind, E. Faxen, and J. Karlsson. Acute rupture of tendo achillis: A prospective, randomised study of comparison between surgical and non-surgical treatment. *J Bone Joint Surg Br*, 83-B(6):843–848, 2001.

[27] M. Myerson. Achilles tendon ruptures. *Inst course Lect.*, 48:219–230, 1999.

[28] J. Leppilahti, S. Orava, and J. Karpakka. Overuse injuries of the achilles tendon. *Ann Chir Gynaecol*, 80(2):202–207, 1991.

[29] Bert R. Mandelbaum, Mark S. Myerson, and Robert Forster. Achilles Tendon Ruptures: A New Method of Repair, Early Range of Motion, and Functional Rehabilitation. *The American Journal of Sports Medicine*, 23(4):392–395, July 1995.

[30] Ren Cetti, Steen-Erik Christensen, Rolf Ejsted, Niels Melchior Jensen, and Uffe Jorgensen. Operative versus nonoperative treatment of Achilles tendon rupture. *The American Journal of Sports Medicine*, 21(6):791–799, December 1993.

[31] H. Kvist and M. Kvist. The operative treatment of chronic calcaneal paratenonitis. *J Bone Joint Surg Br*, 62(3):353 – 357, 1980.

[32] M. Paavola, P. Kannus, and T. Paakkala. Long term prognosis of patients with achilles tendinopathy. *Am J SPorts Med*, 28(5):634 – 642, 2001.

[33] J. Lim, R. Dalal, and M. Waseem. Percutaneous vs. open repair of the ruptured achilles tendon: A prospective randomized controlled study. *Foot Ankle Int.*, 227:559–568, 2001.

[34] Vittorino Testa, Murali K Sayana, Jonathan S Young, and Nicola Maffulli. Percutaneous longitudinal tenotomy in chronic achilles tendonitis. *Bulletin - Hospital for Joint Diseases*, 54(4):241 – 244, 1996.

[35] Testa V., G. Capassso, and N. Maffulli. Ultrasound guided percutaneous longitudianl tenotomy for the management of patellar tendinopathy. *Med Sci Sports Exerc*, 31(11):1509 – 1515, 1999.

[36] R.M. Aspden. Relation between structure and mechanical behaviour of fibre-reinforced composite materials at large strains. *Proceedings of The Royal Society of London, Series A: Mathematical and Physical Sciences*, 406(1831):287 – 298, 1986.

[37] Y. Lanir. Constitutive equations for fibrous connective tissues. *Journal of Biomechanics*, 16(1):1 – 12, 1983.

[38] J.F.M. Manschot and A.J.M. Brakkee. The measurement and modelling of the mechanical properties of human skin in vivo. ii. the model. *Journal of Biomechanics*, 19(7):517–21, 1986.

[39] E.J. Cummins, B.J. Anson, B.W. Car, R.R. Wright, and E.D.W. Hauser. The structure of the calcaneal tendon (of achilles) in relation to orthopedic surgery. *Surg Gynecol Obstet*, pages 107 – 116, 1946.

[40] S. Koch and B. Tillmann. Anatomical comment structure of the gastrocnemius tendon. *Orthopedics and Traumatology*, 4(3):184–185, 1995.

[41] Andrew D. Waggett, James R. Ralphs, Alvin P. L. Kwan, David Woodnutt, and Michael Benjamin. Characterization of collagens and proteoglycans at the insertion of the human achilles tendon. *Matrix Biology*, 16(8):457 – 470, 1998.

[42] A. Viidik. Tensile strength properties of achilles tendon systems in traineds and untrained rabbits. *Acta Orthop Scand*, 10:261–272, 1962.

[43] Y.C. Fung, N. Perrone, and M. Anliker. *Biomechanics: Its Foundations and Objectives*, chapter Stress strain history relations of soft tissues in simple elongation, pages 181–208. Englewood Cliffs, NJ: Prentice-Hall, 1972.

[44] DE Birk, JM Fitch, JP Babiarz, KJ Doane, and TF Linsenmayer. Collagen fibrillogenesis in vitro: interaction of types I and V collagen regulates fibril diameter. *J Cell Sci*, 95(4):649–657, 1990.

[45] M. Benjamin, P. Theobald, D. Suzuki, and H. Toumi. The anatomy of the achilles tendon. In N. Maffulli and C. Almekinders, editors, *The Achilles Tendon*. Springer, 2007.

[46] SL. Woo and E. Young. *Basic Orthopaedic Biomechanics*, chapter Structure and function of tendons and ligaments, pages 199–243. Raven Press: New York, 1991.

[47] S L Y Woo, G A Johnson, and B A Smith. Mathematical modeling of ligaments and tendons. *Journal of Biomechanical Engineering*, 115:468–473, 1993.

[48] P. Kannus and L. Jozsa. Histopathological changes preceding spontaneous rupture of a tendon: A controlled study of 891 patients. *J Bone Joint Surg Am*, 73(10):1507–1525, 1991.

[49] B Huffard, P F O Loughlin, T Wright, J Deland, and J G Kennedy. Achilles tendon repair : Achillon system vs . Krackow suture : An anatomic in vitro biomechanical study. *Clinical Biomechanics*, 23(9):1158–1164, 2008.

[50] CA. Soma and BR. Mandelbaum. Achilles tendon disorders. *Clinics in Sports Medicine*, 1994.

[51] T A Wren, S A Yerby, G S Beaupre, and D R Carter. Mechanical properties of the human achilles tendon. *Clin. Biomech.*, 16:245–251, 1998.

[52] A.A.H.J. Sauren, M.C. van Hout, A.A. van Steenhoven, F.E. Veldpaus, and J.D. Janssen. The mechanical properties of porcine aortic valve tissues. *Journal of Biomechanics*, 16(5):327 – 337, 1983.

[53] S. L.-Y. Woo, B. R. Simon, S. C. Kuei, and W. H. Akeson. Quasi-linear viscoelastic properties of normal articular cartilage. *Journal of Biomechanical Engineering*, 102(2):85–90, 1980.

[54] E. O. Carew, E. A. Talman, D. R. Boughner, and I. Vesely. Quasi-linear viscoelastic theory applied to internal shearing of porcine aortic valve leaflets. *Journal of Biomechanical Engineering*, 121(4):386–392, 1999.

[55] L J Dortmans, A A van de Ven, and A A Sauren. A note on the reduced creep function corresponding to the quasi-linear visco-elastic model proposed by fung. *J Biomech Eng*, 116(3):373–5, 1994.

[56] M.K. Kwan, H.T.C. Lin, and S L Woo. On the Viscoelastic Properties of the Anteromedial Bundle of the Anterior Cruciate Ligament. *J. Biomech*, 26:447–452, 1993.

[57] T.C. Doehring, E. Carew, and I. Vesely. The effect of strain rate on the viscoelastic response of aortic valve tissue : A direct-fit approach. *Annals of Biomedical Engineering*, 32(2):223–232, 2004.

[58] B T Haraldsson, P Aagaard, M Krogsgaard, T Alkjaer, M Kjaer, and S P Magnusson. Region-specific mechanical properties of the human patella tendon Region-specific mechanical properties of the human patella tendon. *Journal of Applied Physiology*, pages 1006–1012, 2005.

[59] G A Johnson, D M Tramaglini, R E Levine, K Ohno, N Y Choi, and S L Woo. Tensile and viscoelastic properties of human patellar tendon. *J Orthop Res*, 12:796–803, 1994.

[60] N D Reeves, C N Maganaris, and M V Narici. Effect of strength training on human patella tendon mechanical properties of older individuals. *J. Physiol*, 548(3):971–981, 2007.

[61] Keitaro Kubo, Hiroaki Kanehisa, and Tetsuo Fukunaga. Effects of resistance and stretching training programmes on the viscoelastic properties of human tendon structures in vivo. *J. Physiol*, 538(1):219–226, 2002.

[62] G. Lewis and KM. Shaw. Modeling the tensile behavior of human achilles tendon. *Biomed Mater Eng.*, 7(4):231–244, 1997.

[63] O. Basso, A.A. Amis, A. Race, and D.P. Johnson. Patellar tendon fiber strains: their differential responses to quadriceps tension. *Clin Orthop Relat Res*, 400:246–253, 2002.

[64] F. Iaconis, R. Steindler, and G. Marinozzi. Measurements of cross-sectional area of collagen structures (knee ligaments) by means of an optical method. *Journal of Biomechanics*, 20(10):1003 – 1007, 1009–1010, 1987.

[65] S.L. Woo, M.I. Danto, K.J. Ohland, T.Q. Lee, and P.O. Newton. The use of a laser micrometer system to determine the cross-sectional shape and area of ligaments: a comparative study with two existing methods. *J Biomech Eng.*, 112(4):426–431, 1990.

[66] M. Noguchi, T. Kitura, K. Ikoma, and Y. Kusaka. A method of in-vitro measurement of the cross-sectional area of soft tissues, using ultrasonography. *J Orthop Sci*, 7:247 – 251, 2002.

[67] C. Gillis, N. Sharkey, S.M. Stover, R.R. Pool, D.M. Meagher, and N. Willits. Ultrasonography as a method to determine tendon cross-sectional area. *Am J. Vet Res.*, 56(10):1270–1274, 1995.

[68] Amos Race and Andrew A Amis. Cross-sectional area measurement of soft tissue. a new casting method. *J. Biomech*, 29(9):1207–1212, 1996.

[69] David L. Butler, Matthew D. Kay, and Donald C. Stouffer. Comparison of material properties in fascicle-bone units from human patellar tendon and knee ligaments. *Journal of Biomechanics*, 19(6):425 – 432, 1986.

[70] J. Shi and C. Tomasi. Good features to track. In *IEEE Conference on Computer Vision and Pattern Recognition*, 1994.

[71] H.R. Screen, D.A. Lee, D.L. Bader, and J.C. Shelton. An investigation into the effects of the hierarchical structure of tendon fascicles on micromechanical properties. *Proc Inst Mech Eng H.*, 218(2):109–119, 2004.

[72] T.C. Doehring, M. Kahelin, and I. Vesely. Direct measurement of nonuniform large deformations in soft tissues during uniaxial extension. *Journal of Biomechanical Engineering*, 131(6):061001, 2009.

[73] W Yang, T C Fung, K S Chian, and C K Chong. Viscoelasticity of esophageal tissue and application of QLV model. *J. Biomech. Eng.*, 128(6):909–916, 2006.

[74] S.D. Abramowitch, S.L.-Y. Woo, T.D. Clineff, and R.E. Debski. An evaluation of the quasilinear viscoelastic properties of the healing medial collateral ligament in a goat model. *Annals of Biomedical Engineering*, 32(3):329 – 35, 2004.

[75] J.R. Funk, G.W. Hall, J.R. Crandall, and W.D. Pilkey. Linear and quasi-linear viscoelastic characterization of ankle ligaments. *Transactions of the ASME. Journal of Biomechanical Engineering*, 122(1):15 – 22, 2000.

[76] Y.C. Fung. *Biomechanics: mechanical properties of living tissues*, volume 2nd ed. New York: Springer-Verlag, 1993.

[77] P. Kannus. Structure of the tendon connective tissue. *Scandinavian Journal of Medicine and Science In Sports*, 10(6):312–320, 2000.

[78] T.S. Atkinson, R.C. Haut, and N.J. Altiero. A poroelastic model that predicts some phenomenological responses of ligaments and tendons. *Transactions of the ASME. Journal of Biomechanical Engineering*, 119(4):400 – 5, 1997.

[79] S.L. Butler, S.s. Kohles, R.J. Thielke, C. Chen, and Jr. Vanderby, R. Interstitial fluid flow in tendons or ligaments: a porous medium finite element simulation. *Med. Biol. Eng. Comput. (UK)*, 35(6):742 – 6, 1997.

[80] P. Vena. A computational model of viscoelastic composite materials for ligament or tendon prostheses. *Advanced Composites Letters*, 9(3):181 – 192, 2000.

[81] M.E. Zobitz, Z.-P. Luo, and K.-N. An. Determination of the compressive material properties of the supraspinatus tendon. *Journal of Biomechanical Engineering*, 123(1):47 – 51, 2001.

[82] CGAL, Computational Geometry Algorithms Library. http://www.cgal.org.

[83] Per-Olof. Persson and Gilbert. Strang. A simple mesh generator in matlab. *SIAM Review*, 46(2):329–345, June 2004.

[84] Luzhong Yin and Dawn M. Elliott. A biphasic and transversely isotropic mechanical model for tendon:: application to mouse tail fascicles in uniaxial tension. *Journal of Biomechanics*, 37(6):907 – 916, 2004.

Vita

OLUSEENI A. KOMOLAFE

EDUCATION

Ph.D.	Drexel University	Biomedical Engineering	SEPTEMBER 2010
B.Sc.	University of Maryland, Baltimore County	Mechanical Engineering	MAY 2005

RESEARCH EXPERIENCE

- Drexel University - Research Assistant
  Computational Imaging and Biomechanical Laboratory
  (P.I./Advisor – Todd C. Doehring, Ph.D.)

- Alfred I. DuPont Hospital for Children - Research Assistant
  Pediatric Engineering Research Laboratory
  (P.I. – Tariq Rahman, Ph.D.)

TEACHING EXPERIENCE

Undergraduate Courses	Graduate Courses
BMES 212: The Body Synthetic	BMES 641: Biomechanics I
BMES 301: Experimental Biomechanics	BMES 642: Biomechanics II
BMES 440: Introduction to Biodynamics	BMES 643: Biomechanics III

PUBLICATIONS/CONFERENCE PAPERS

- **Komolafe, O.A., Doehring, T.C.** (2010) Fascicle scale loading and failure behavior of the Achilles tendon. J.Biomech. Eng. Vol 132: 021004(1-5)

- **Komolafe, O.A., Doehring, T.C.** A load-direction dependent QLV model for fascicle-scale mechanical tests of soft collagenous tissues. In review

- **Komolafe, O.A., Doehring, T.C.** On the bidirectional viscoelastic behavior of the human Achilles Tendon, Proceedings of the ASME Summer Bioengineering Conference, SBC 2008, Part B, p 821 - 822, 2009.

- **Komolafe, O.A., Doehring, T.C.** Nonlinear elastic behavior of the Achilles tendon at the fascicle scale. Proceedings of the ASME Summer Bioengineering Conference, SBC 2007, p 975-976, 2007.